

# Optical polarimetry of cataclysmic variables

Claudia V. Rodrigues

INPE (National Institute of Space Research)

Brazil

[claudia.rodrigues@inpe.br](mailto:claudia.rodrigues@inpe.br)

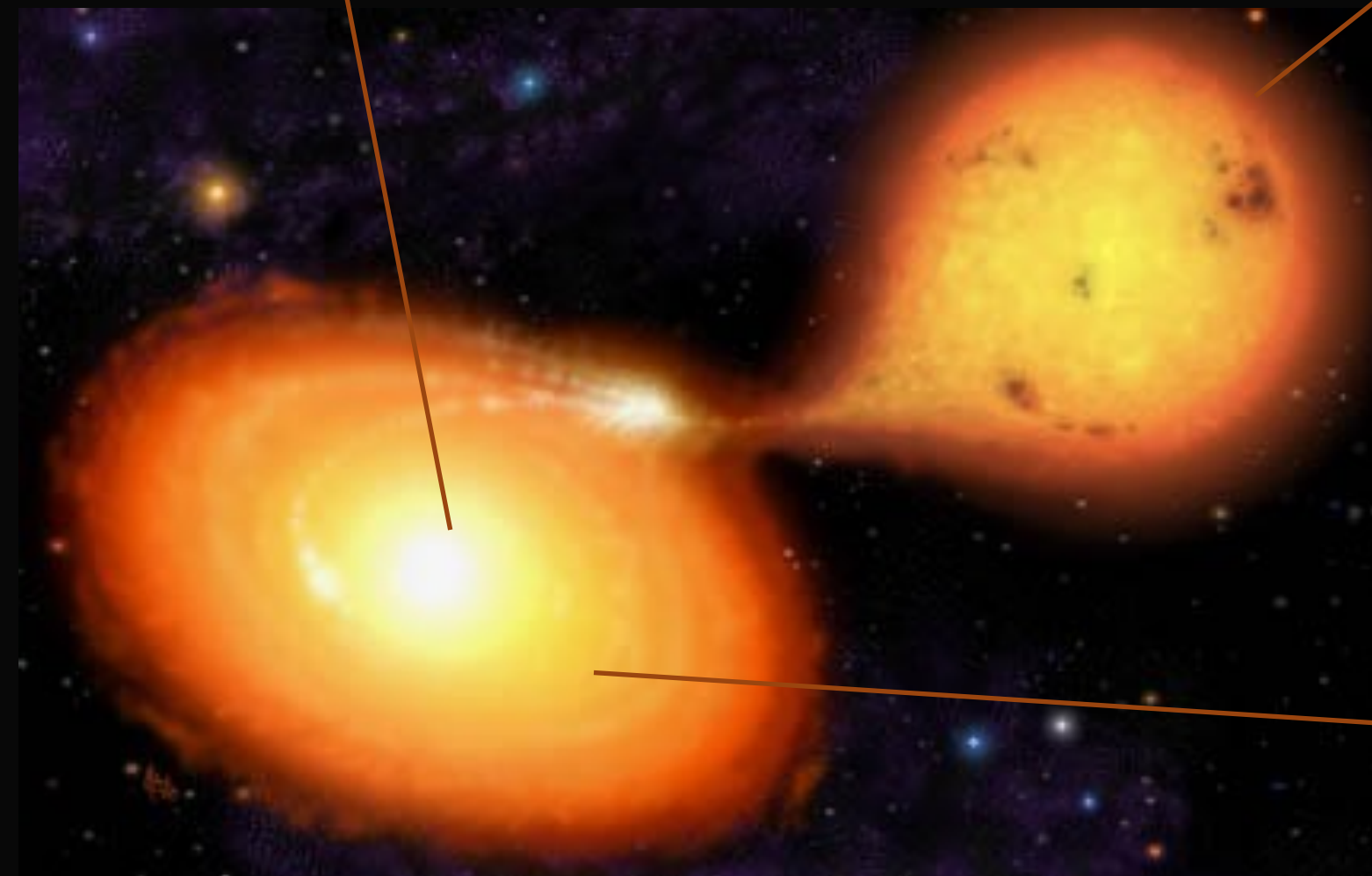
# SUMMARY

---

- What is a cataclysmic variable?
  - ❖ When its emission can be polarized?
- Measurements of polarization and magnetic accretion in CVs
- Getting physical information from polarimetric measurements

# CATAclysmic VARIABLES

White dwarf (WD)



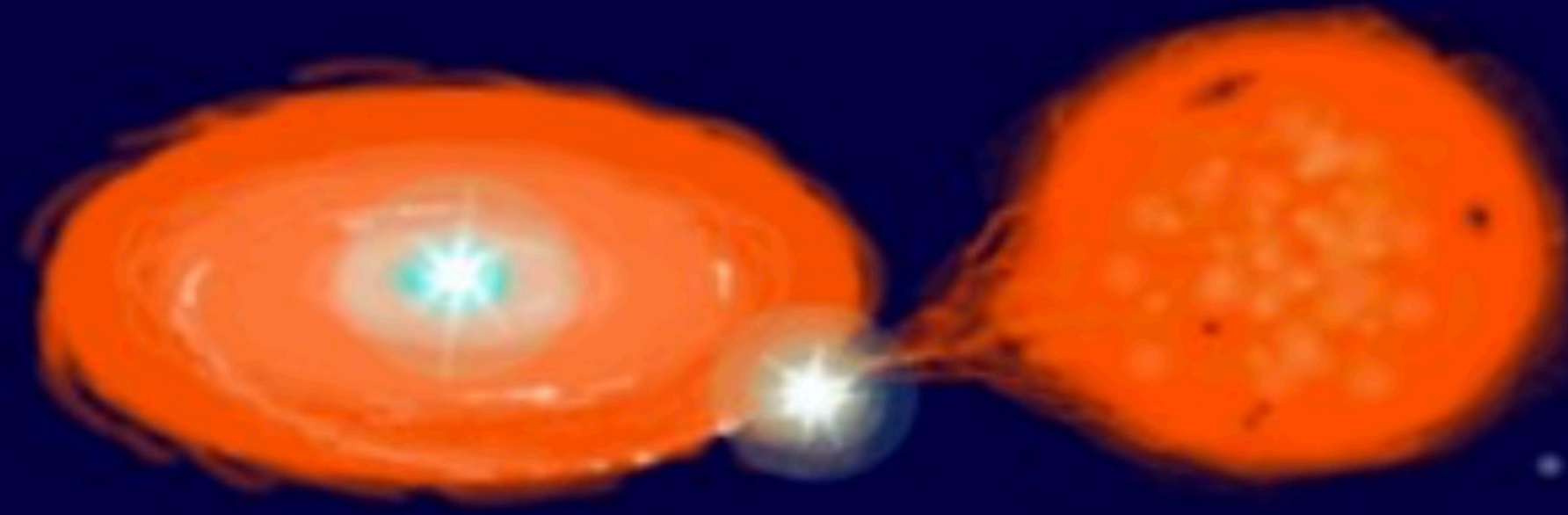
main sequence  
or slightly  
evolved  
low mass star

Accretion disk

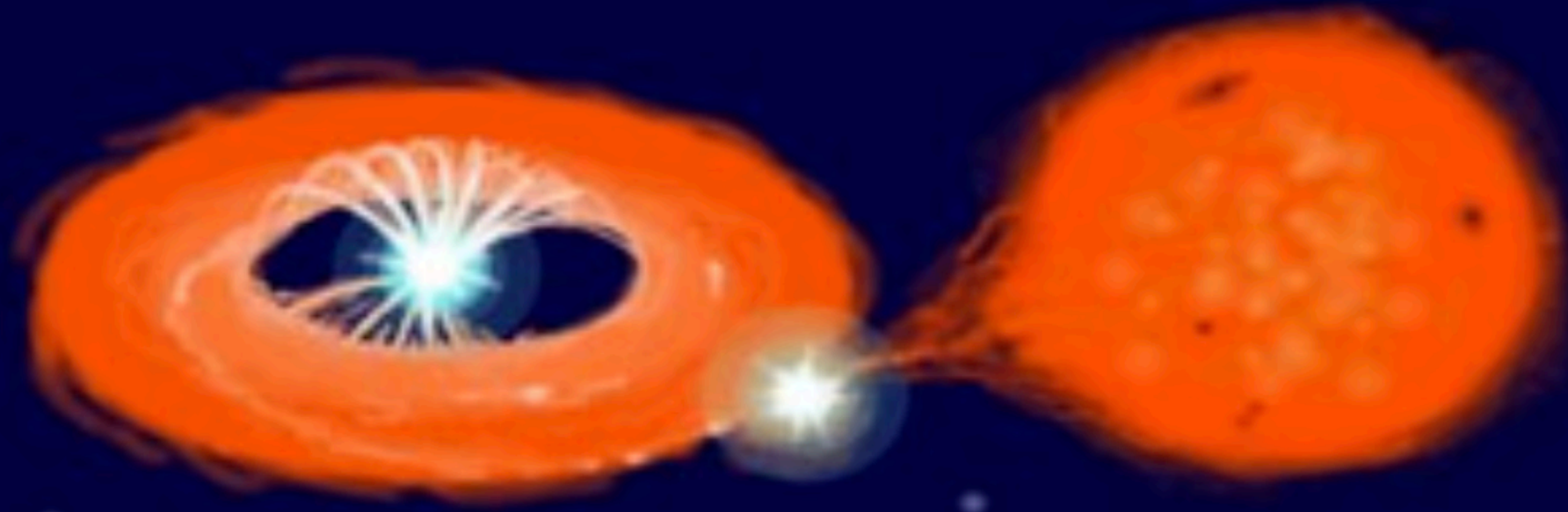
# CV ACCRETION GEOMETRY

---

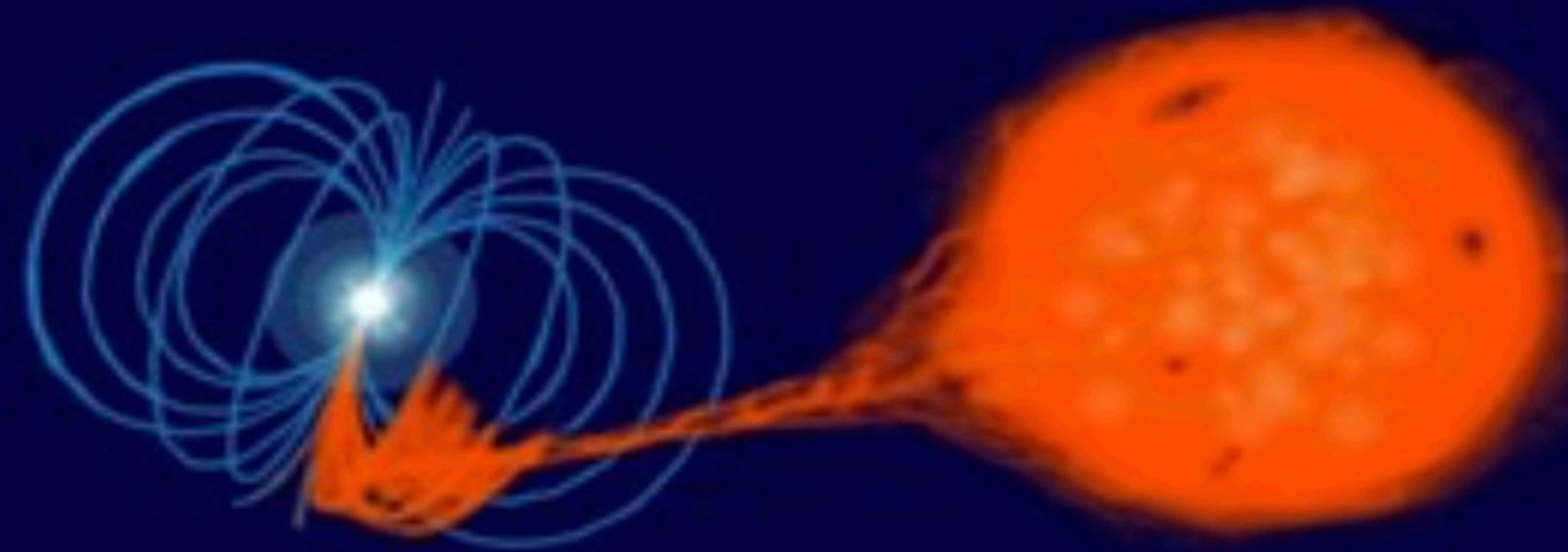
- The white dwarf can have a magnetic field intense enough to have a role in the accretion geometry and emitted (polarized) radiation.



Non-magnetic CV



Intermediate polar



Polar

Magnetic CVs

# CV ACCRETION GEOMETRY

---

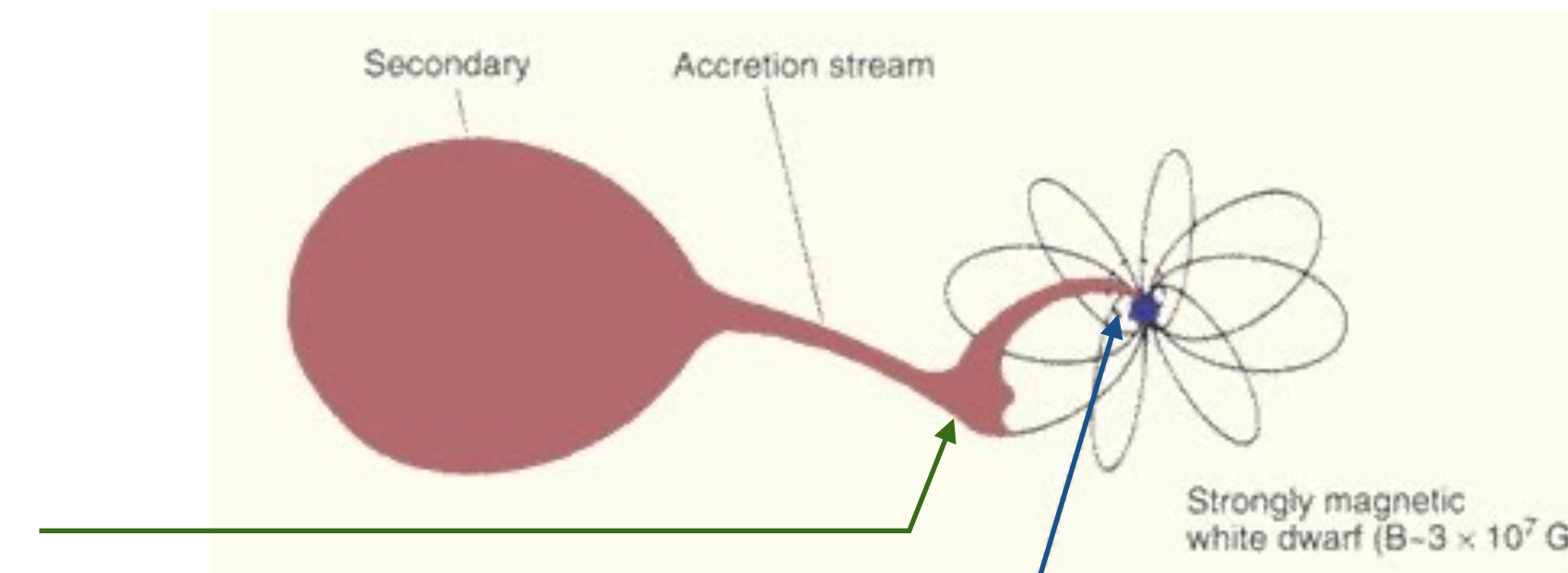
- The white dwarf can have a magnetic field intense enough to have a role in the accretion geometry and emitted (polarized) radiation.
- The accretion geometry is a function of the magnetosphere radius, which depends on:
  - ❖ the white-dwarf magnetic field;
  - ❖ the mass-transfer rate;
  - ❖ the white-dwarf mass (more restricted than the above parameters).

**Alfven radius**  $r_A = \left( \frac{\mu^4}{2GM\dot{M}^2} \right)^{1/7}$

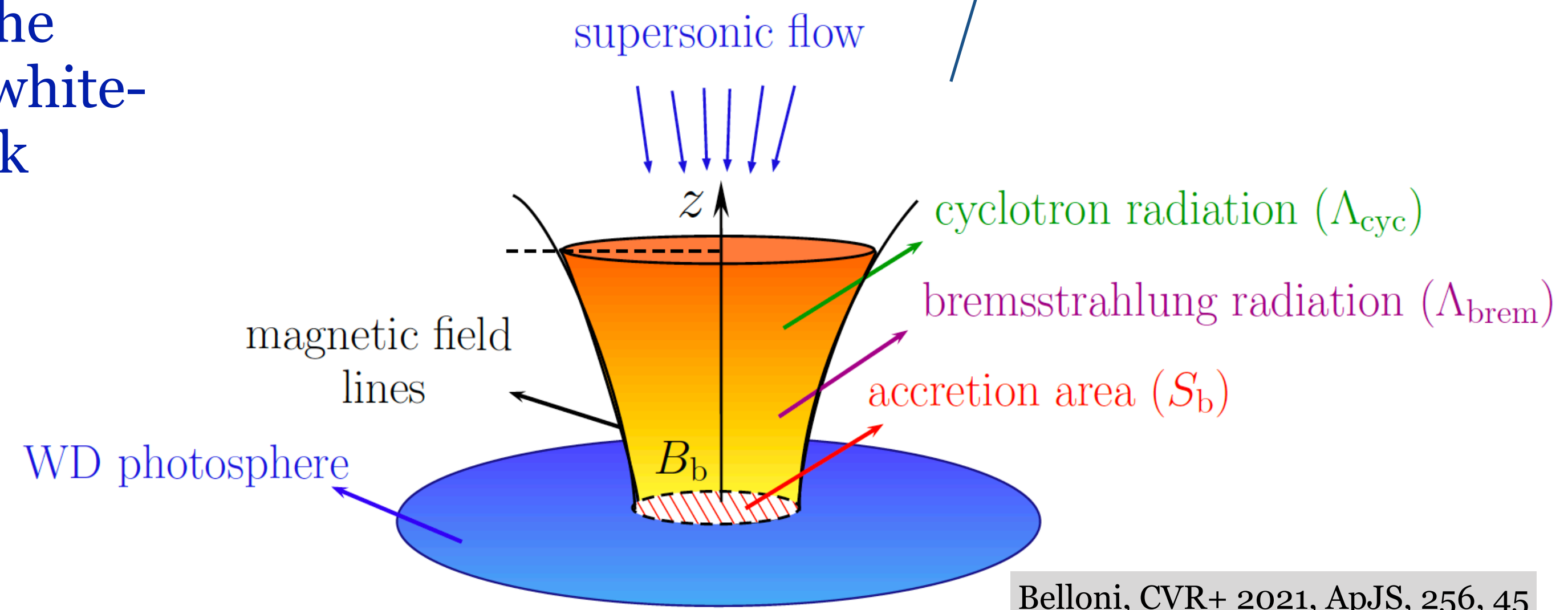
# MAGNETIC ACCRETION

<https://heasarc.gsfc.nasa.gov/docs/objects/cvs/cvstext.html>

- In magnetic cataclysmic variables, the mass flow reaches the white dwarf through a **magnetic column**.



- Post-shock region
  - ❖ a density enhancement in the magnetic column near the white-dwarf surface due to a shock

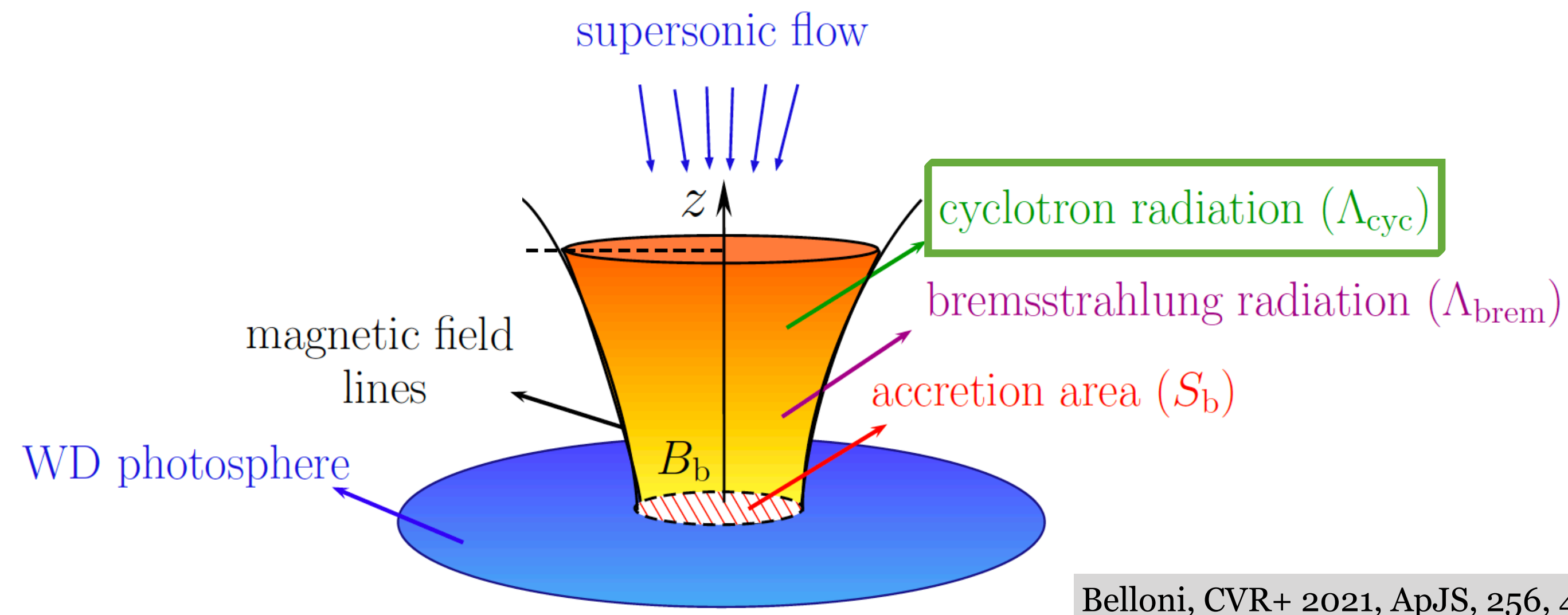


Belloni, CVR+ 2021, ApJS, 256, 45

# ORIGIN OF THE POLARIZATION

---

- The origin of the polarization in magnetic CVs is the cyclotron radiation from the post-shock region:
  - ❖ occurs in optical and infrared wavelengths;
  - ❖ is anisotropic and polarized.
- Polarization can be measured if the emission of the post-shock region is not completely diluted by other components



# VARIABLE POLARIZATION

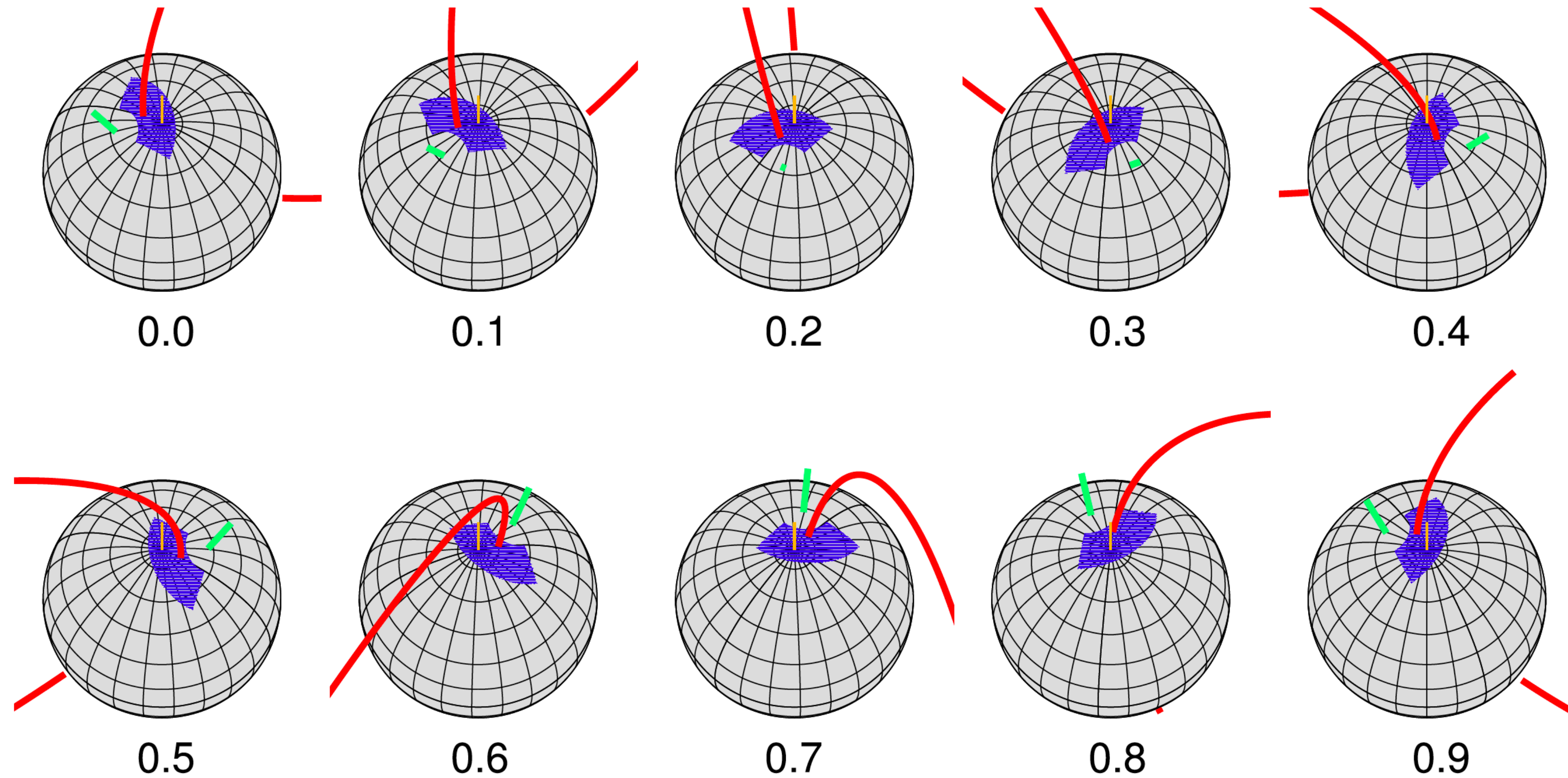


**Figure 11.** Accretion geometry of V348 Pav as seen by the observer in different phases. The 3D PSR on the WD surface is shown in blue. The reference magnetic field line that passes through the central point of the PSR is shown in red. The  $B$ -axis is shown by the green straight line and the WD rotation axis, by the orange line.

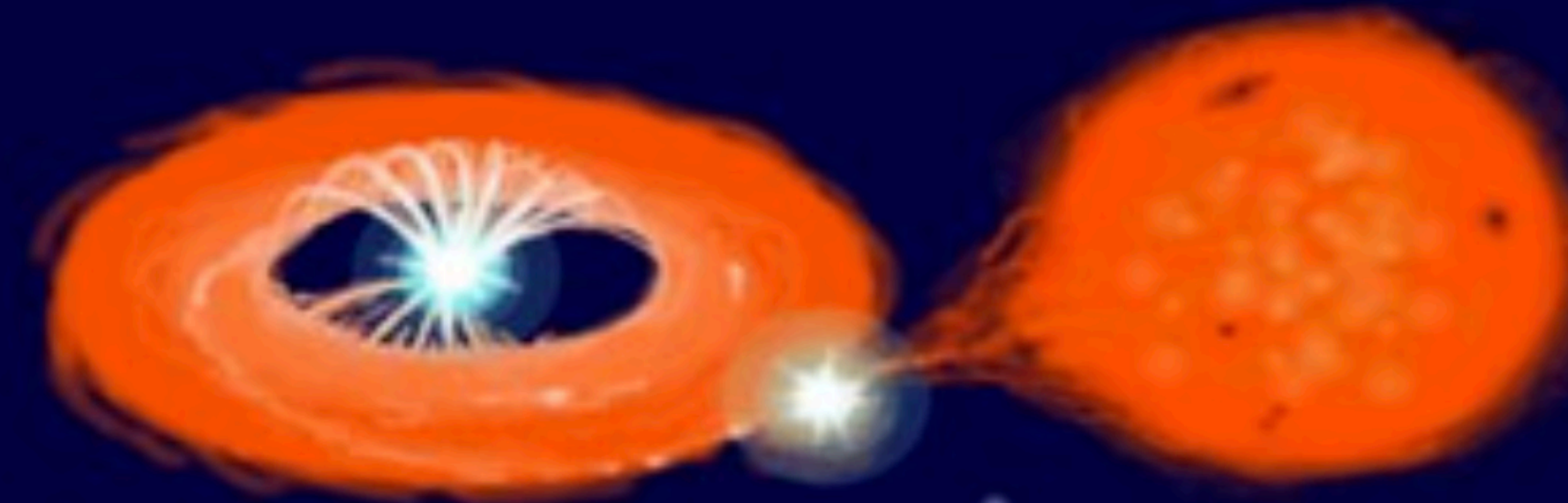
Oliveira, CVR+ 2019, MNRAS, 489, 4032

# **Polarimetric measurements**

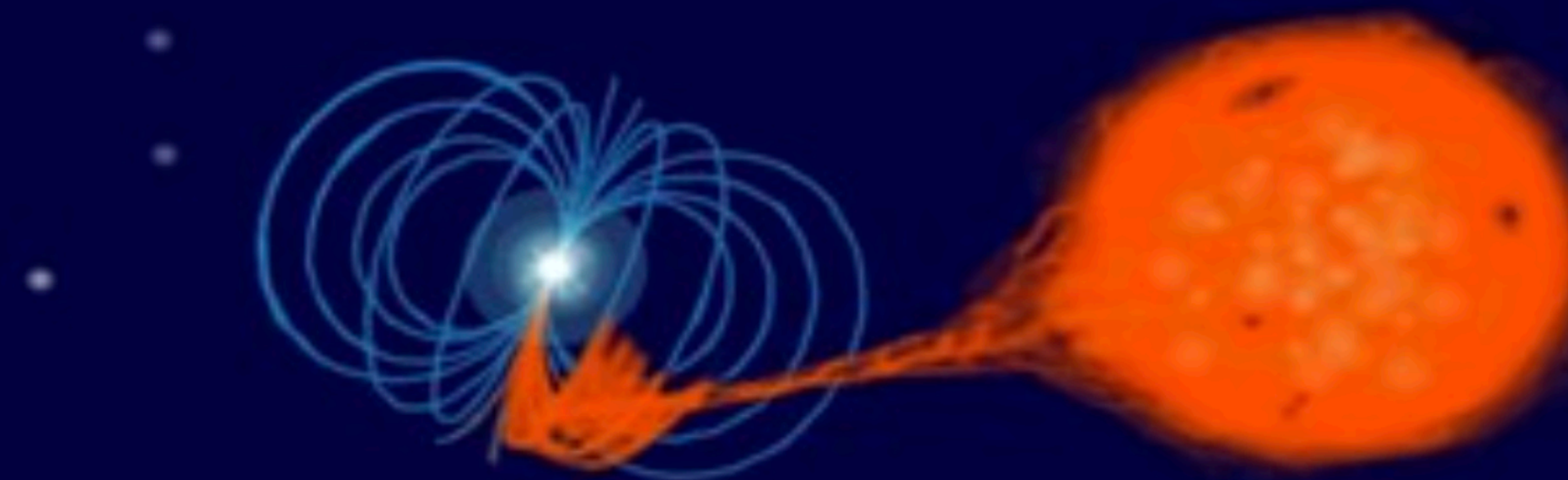
- The optical polarization in magnetic CVs
  - ❖ intermediate polars (DQ Her)
  - ✓ small values of polarization
  - ❖ polars (AM Her)
  - ✓ large values of polarization

Disk dilutes the polarization from the post-shock region

The post-shock region is the main emitting region in the entire system



Intermediate polar



Polar

# POLARIZATION IN IPs

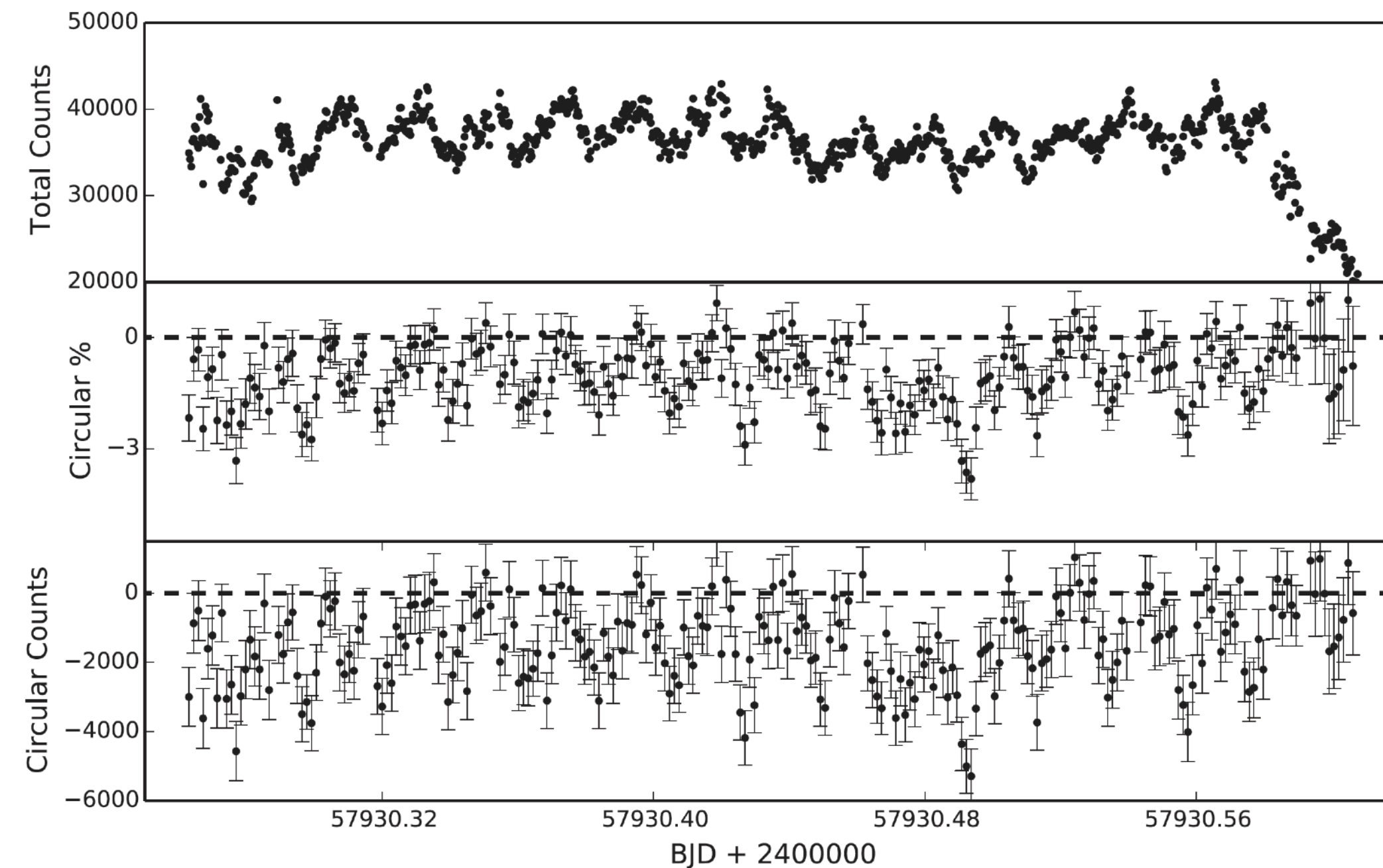
---

A periodic variation of circular polarization is a signature of magnetic accretion in CVs

- Circular optical polarization can be observed in some intermediate polars at a level of around 1%.
  - ❖ Some efforts to measure polarization in large samples
    - ◆ Butters et al., 2009, *A&A*, 496, 891 (Turpol @ 2.56m NOT telescope)
    - ◆ Cropper 1986, *MNRAS*, 222, 225 (UCT polarimeter @ SAAO)
  - ❖ Circular polarization modulated with white-dwarf spin is observed in some IPs

# EXAMPLE OF CIRCULAR POLARIZATION IN IPs

- Nova Sco 1437 = IGR J17014-4306
  - ❖ Instrument: HIPPO, 1.9m at SAAO



Potter & Buckley 2018, MNRAS, 473, 4692

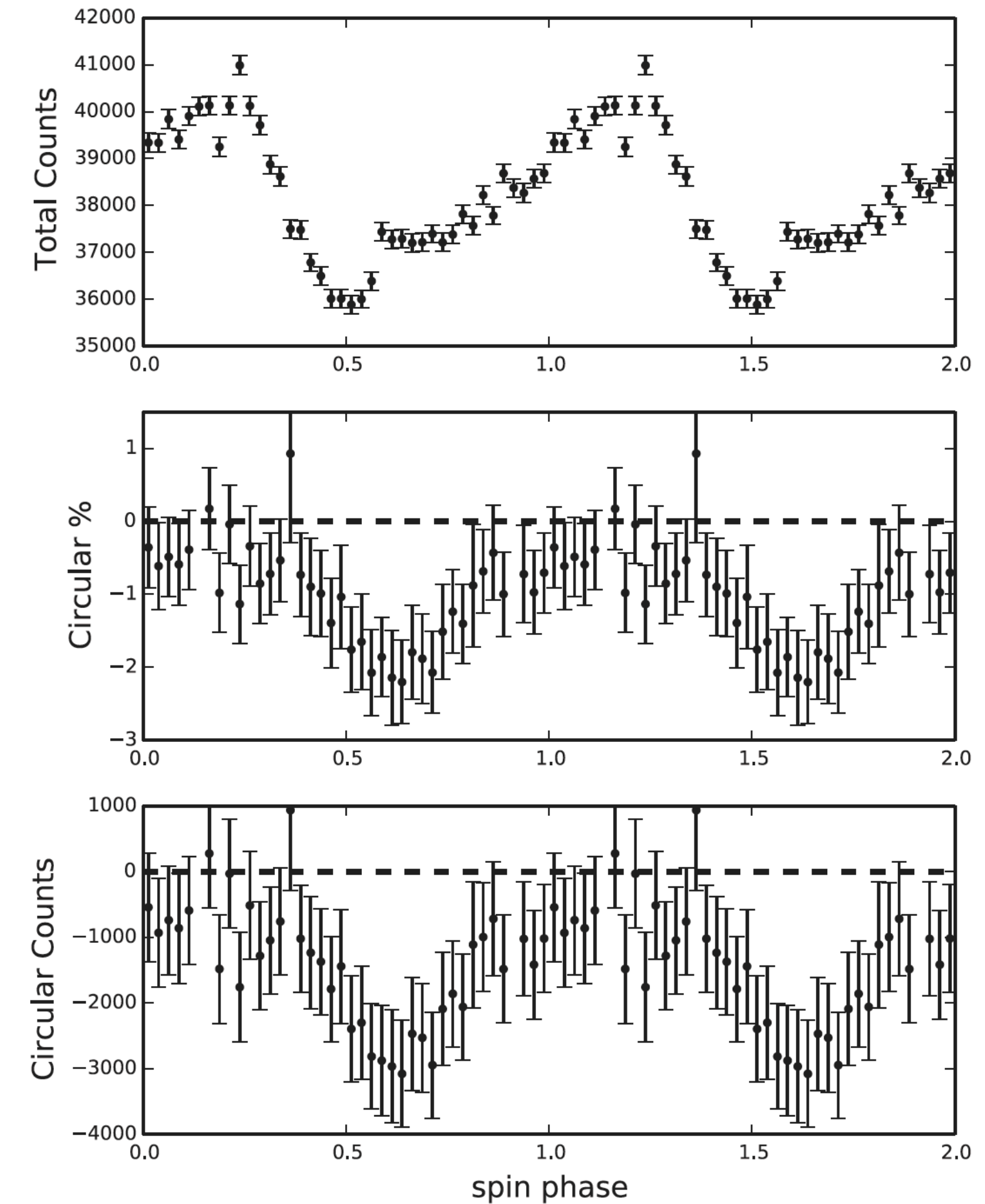


**Figure 3.** Spin-folded photometry and circular polarimetry of the June 25 observations. Bin sizes correspond to  $\sim 46$  s (0.025 spin-phase bins) for the photometry and polarimetry.

# SW SEX SYSTEMS

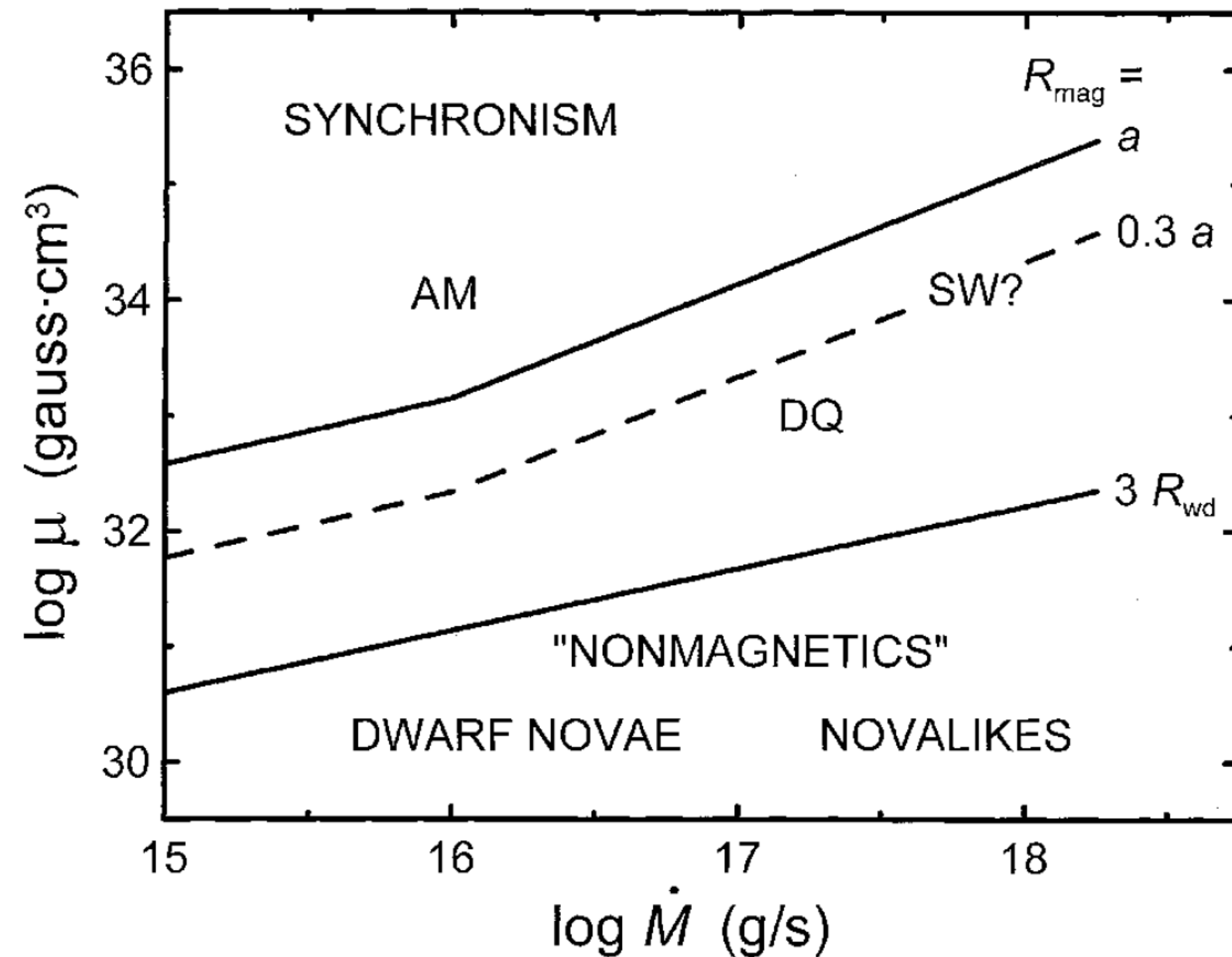


FIG. 16.—Approximate location of magnetic CVs in  $\mu$ - $\dot{M}$  space. The weak dependence on  $m$  and  $m_1$  is ignored ( $=1$ ), and  $P_{\text{orb}}$  is eliminated through an empirical  $\dot{M}(P_{\text{orb}})$  relation. See text for discussion. AM Her stars live above the upper line, and nonmagnetic CVs live below the lower line. DQ Her and SW Sex stars live in between; see text for discussion.

Are the SW Sex systems similar to IPs,  
but with a denser/brighter disk?

Patterson et al. 2002, PASP, 114, 1364

# LS PEG

- LS Peg is a bona-fide SW Sex and observations strongly support magnetic accretion on the white dwarf

ISIS  
4.2 m William  
Herschel

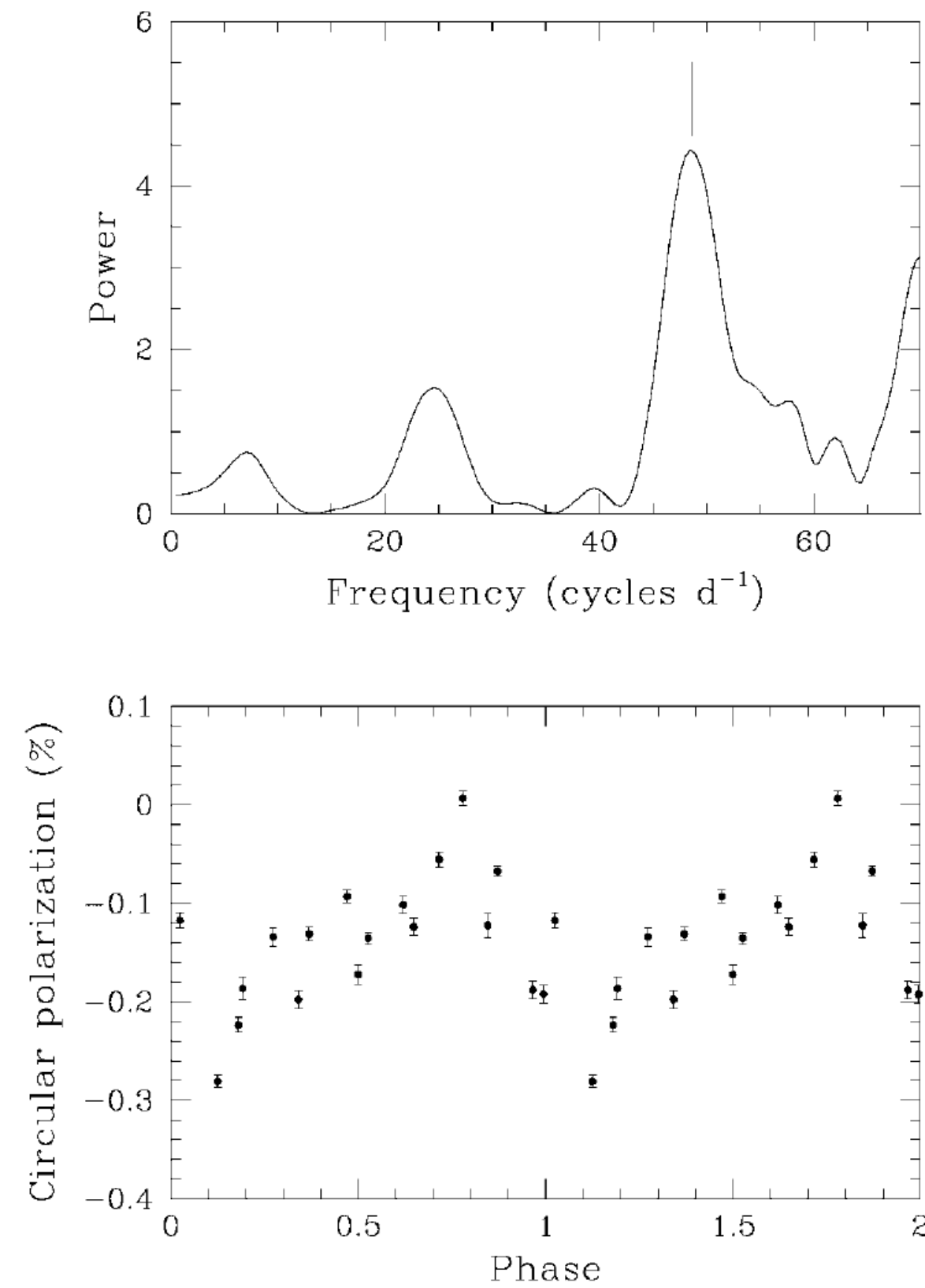
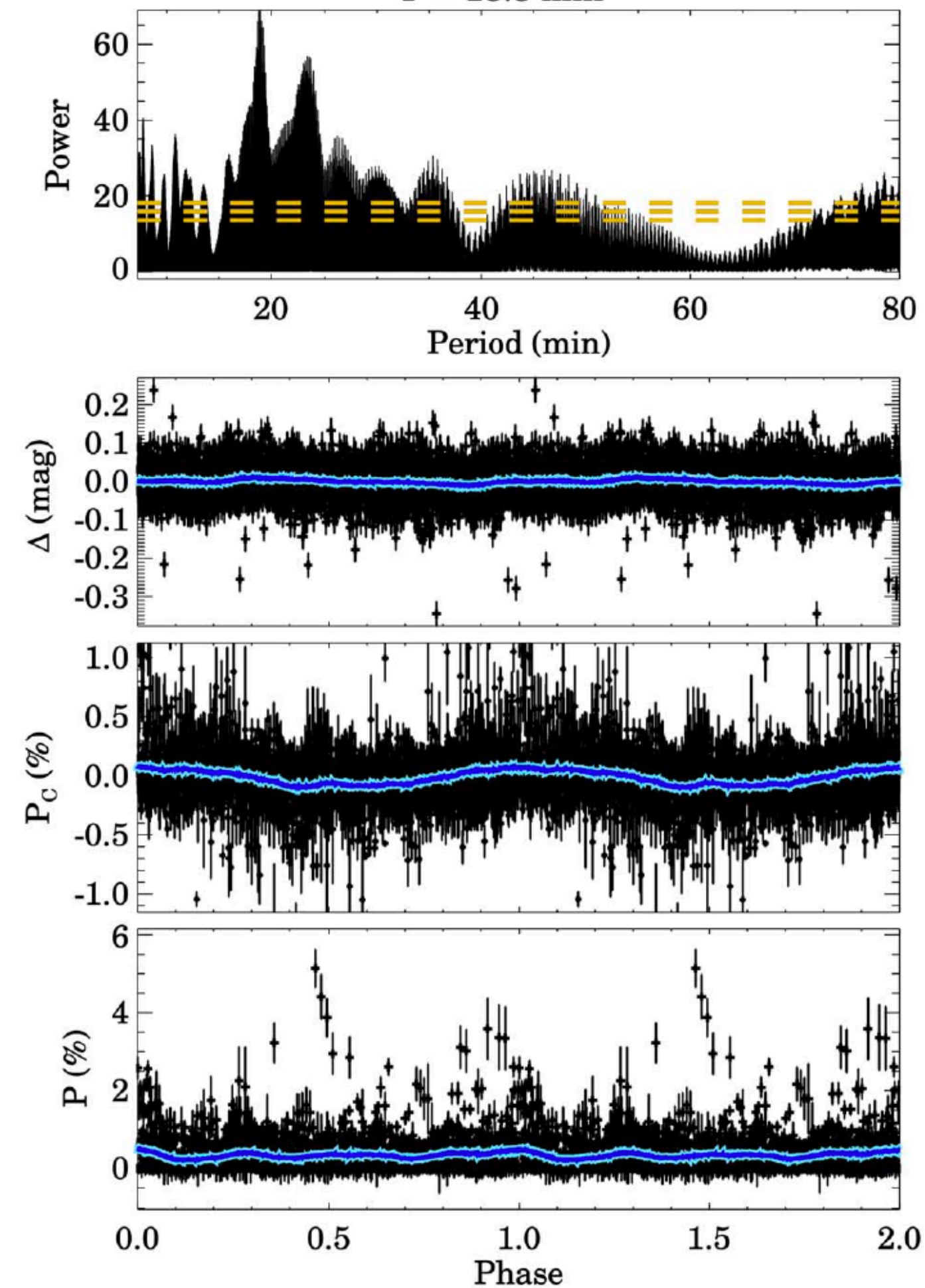


FIG. 3.—*Upper panel:* Power spectrum of the circular polarization data in the B band. The strongest peak at  $\nu_p = 48.7 \pm 3.1 \text{ day}^{-1}$  is marked with a vertical line. *Lower panel:* Circular polarization level in phase with the period  $P_p = 1/\nu_p = 29.6 \pm 1.8$  minutes. Zero phase is arbitrary, and a complete period is repeated for clarity.

LS Peg: Circular Polarization

$P = 18.8 \text{ min}$



IAGPOL  
1.6m OPD

# POLARIMETRY OF SW SEX SYSTEMS

---

- Fractions of positive detection of circular polarization in SW Sex systems (Lima, CVR+ 2021):
  - ❖ 15% in confirmed or candidate SW Sex systems
  - ❖ 30% in confirmed SW Sex systems

The compilation includes measurements having poor time resolution and large errors...

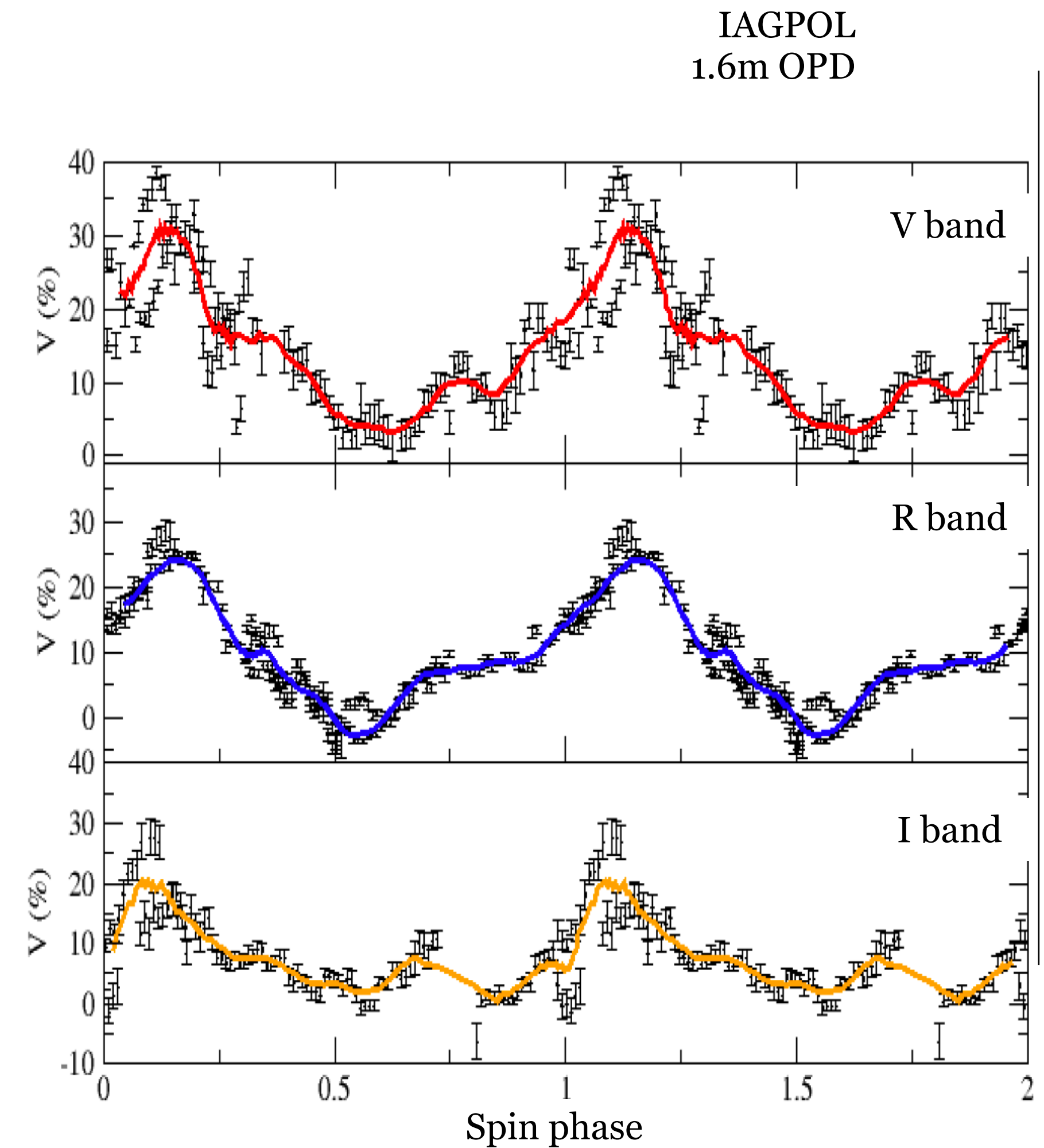
# POLARIZATION OF POLARS

---

- Polars are:
  - ❖ highly polarized objects due to negligible dilution of the post-shock region emission;
  - ❖ excellent laboratories to understand the magnetic accretion on white dwarfs.
- Some examples of measurements of our group in the next slides.

# CRTS J035758.7+102943

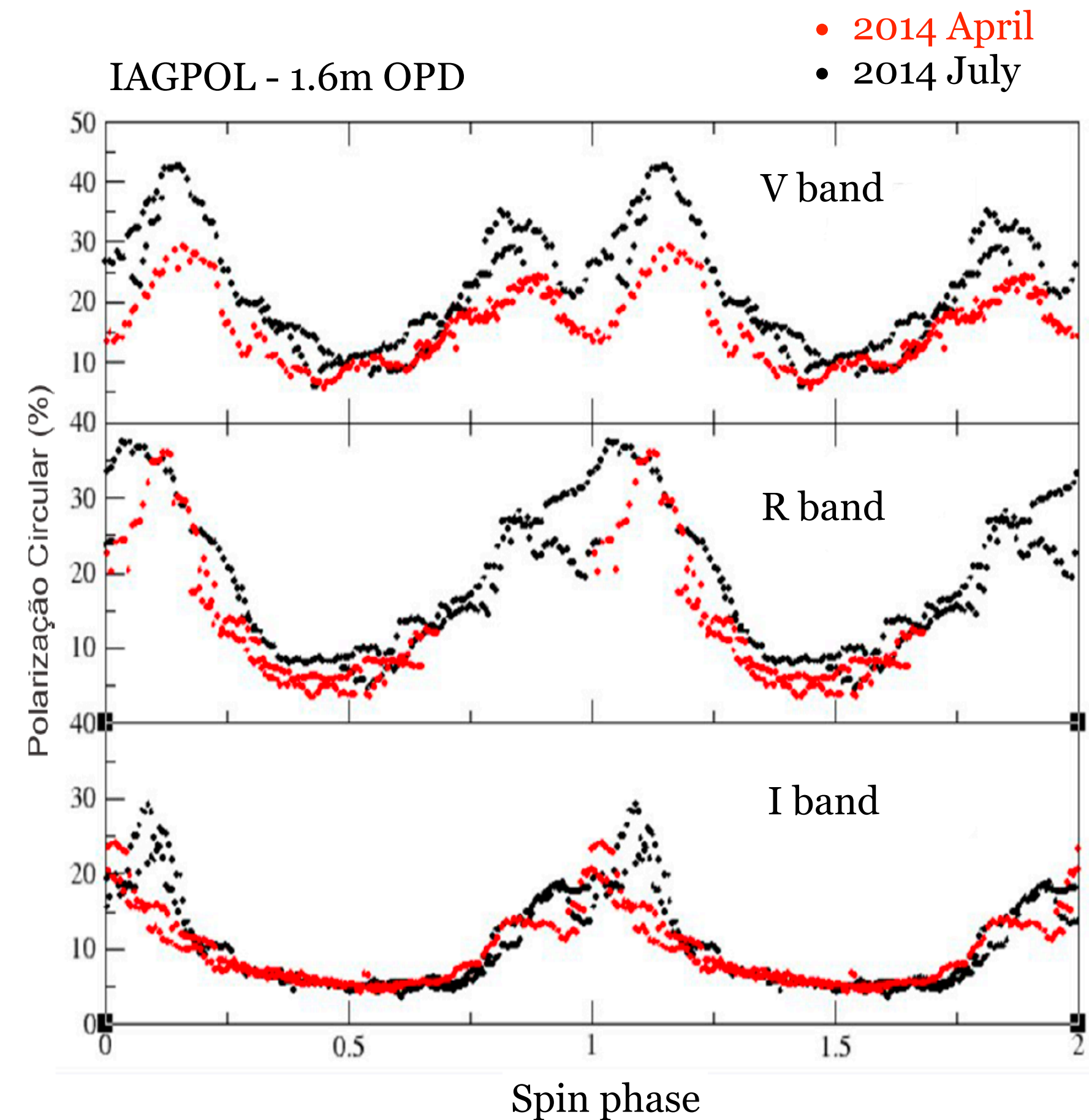
- Transient source of the CRTS
- Polar classification (Schwope & Thinius 2012, AN, 333, 717)
  - ❖ Optical photometry:  $P = 114$  min
  - ❖ XMM source
- Spectroscopy
  - ❖ Thorstensen+2016, AJ, 152, 226
  - ❖ Oliveira, CVR+2017, AJ, 153, 144
- Optical polarimetry (de Souza's Master 2022)



17.5 mag < V < 18.5 mag

# 1RXS J174320.1-042953

- Polar classification
  - ❖ Denisenko & Martinelli (2012)
  - ❖ Oliveira, CVR+2017, AJ, 153, 144
- Polarimetry
  - ❖ Martins's Thesis (2022)



# **Numerical models**

# SOME TOOLS TO MODEL THE POLARIZATION

---

- Wickramasinghe & Meggitt (1985, 1982)
  - ❖ point-like emitting region
  - ❖ cyclotron emission + free-free (=bremsstrahlung) absorption
  - ❖ parameters
    - ◆ electronic temperature,  $T_e$
    - ◆ frequency,  $\omega/\omega_c$
    - ◆ angle between the observer and the magnetic field line,  $\theta$
    - ◆ size parameter,  $\Lambda$  (proportional to  $s N_e B^{-1}$ )
- a table with results allows a straightforward comparison with observations

Meggitt & Wickramasinghe 1982, MNRAS, 198, 71

Wickramasinghe & Meggitt 1985, MNRAS, 214, 605

# DEPENDENCE ON THE VIEWING ANGLE

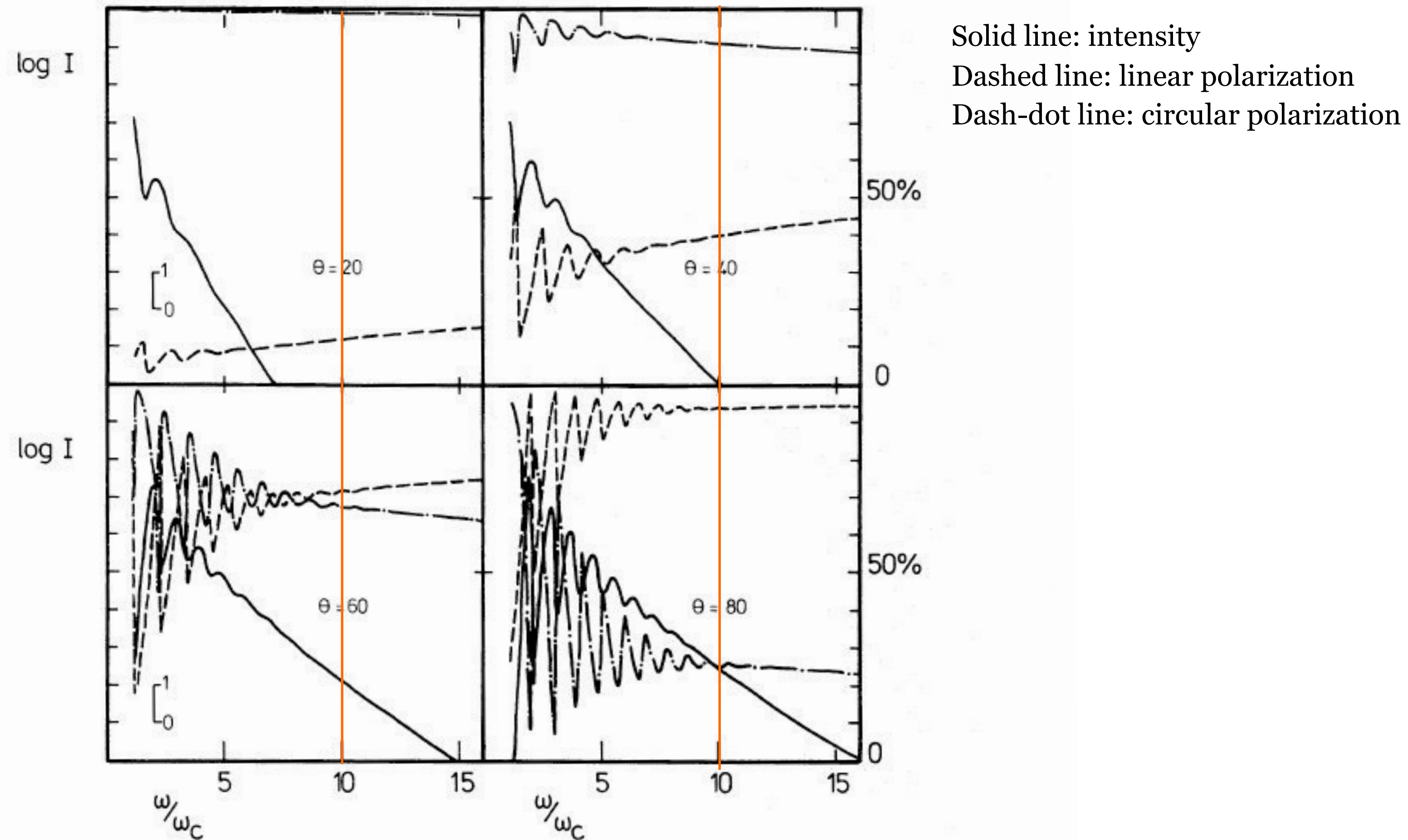


**Figure 2.** The intensity and polarization spectra for optically thin emission at 10 keV at various angles  $\theta$  to the magnetic field. The dash-dot line corresponds to percentage circular polarization and the other lines have the same significance as in Fig. 1.

Meggitt & Wickramasinghe 1982, MNRAS, 198, 71

# EXTENDED EMITTING REGION

- Ferrario & Wickramasinghe (1990, ApJ, 357, 582)
  - ❖ extended, but homogeneous (Ne, Te) arc-shaped emitting (2D) regions
  - ❖ region defined as a ribbon with different lengths in magnetic longitude and latitude

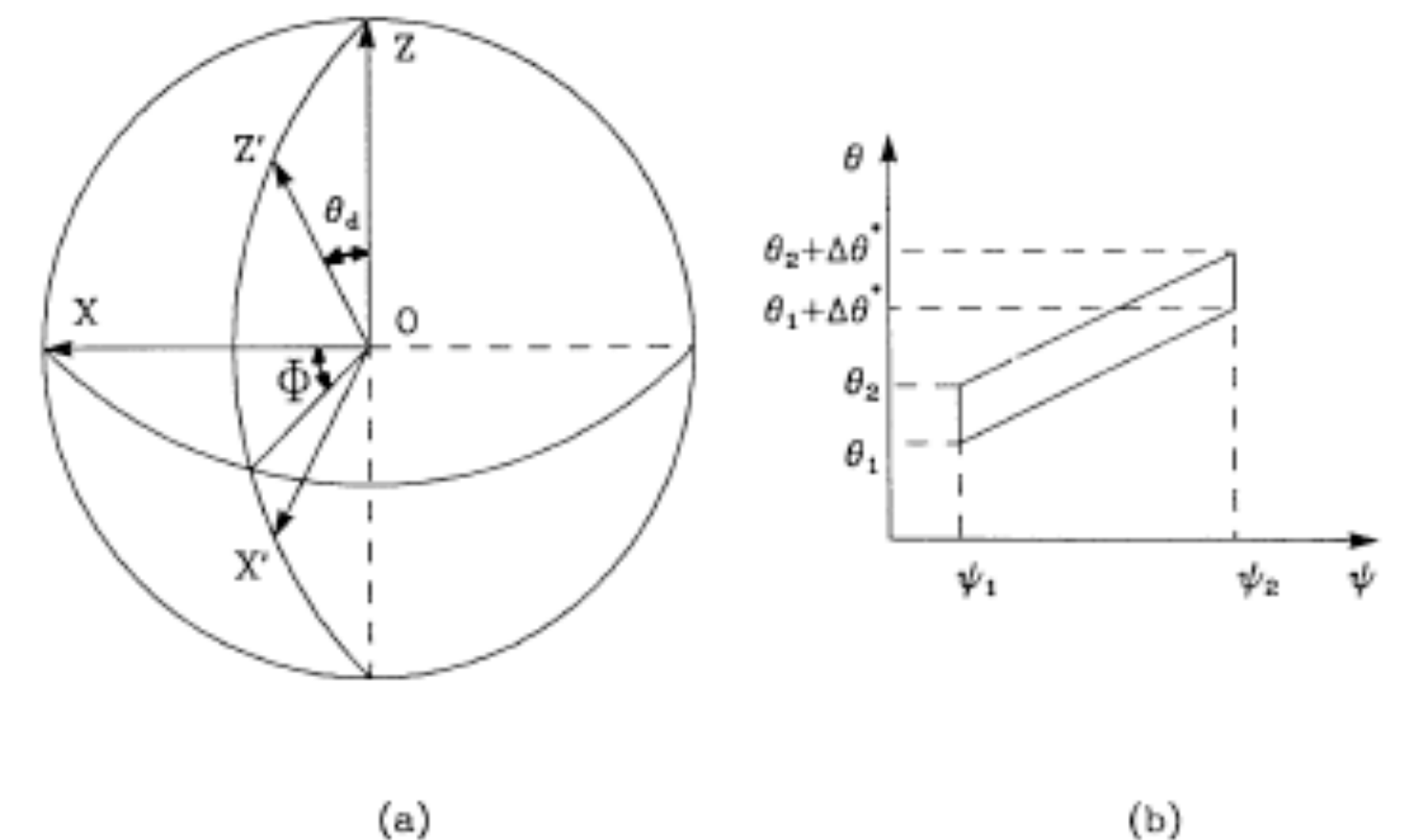


FIG. 1.—(a) White dwarf geometry. The point  $O$  is the center of the white dwarf. The  $z$ -axis is parallel to the rotation axis, and the  $x$ -axis is given by the projection of the line of sight on to the orbital plane. The  $z'$ -axis is parallel to the dipole axis and the  $x'$ -axis is in the plane  $Ozz'$ . The angle that the dipole axis  $z'$  forms with the spin axis  $z$  is indicated by  $\theta_d$ . The angle  $\Phi$  (angle between the projection of the dipole axis  $z'$  on to the orbital plane and the  $x$ -axis) increases or decreases with orbital phase depending on the sense of rotation of the white dwarf. (b) Magnetic longitudinal ( $\psi$ ) and latitudinal ( $\theta$ ) boundaries of the cyclotron emission region.

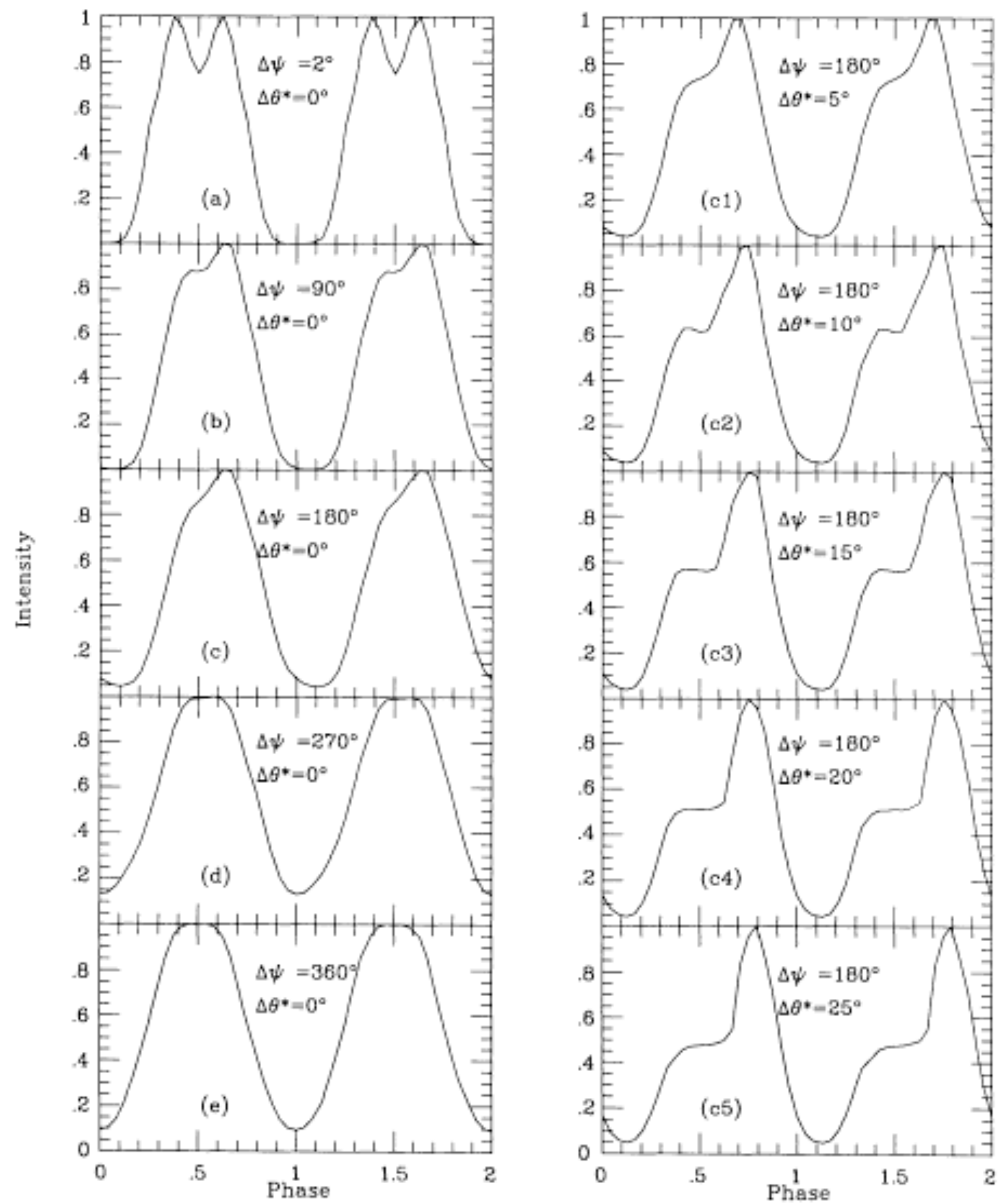


FIG. 2

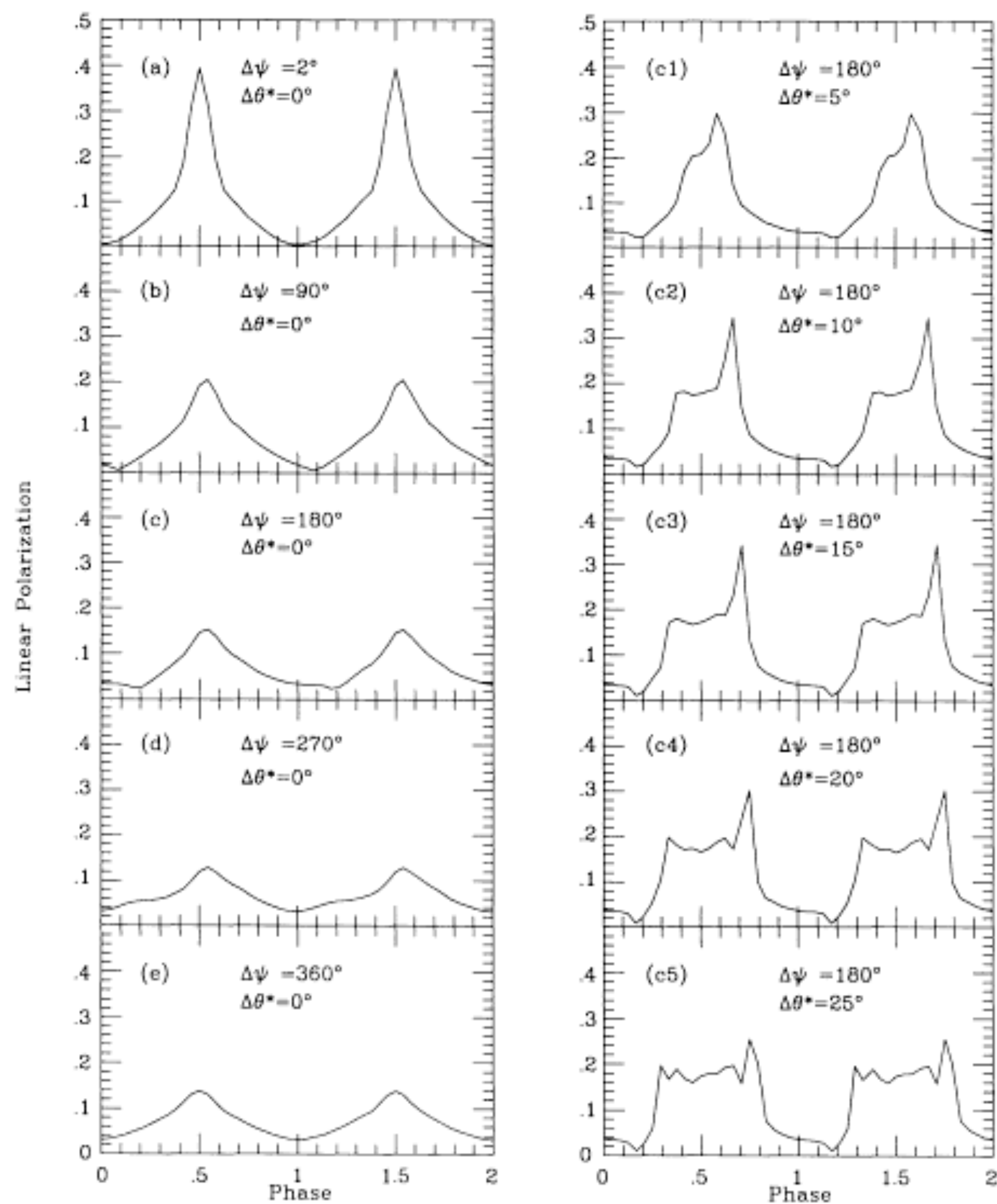


FIG. 3

FIG. 2.—Theoretical intensity curves obtained for fixed values of  $i (= 50^\circ)$ ,  $\theta_A (= 20^\circ)$ , and angular thickness of the cyclotron emission region ( $\theta_1 = 10^\circ$  and  $\theta_2 = 12^\circ$ ).

FIG. 3.—Theoretical linear polarization curves obtained for fixed values of  $i (= 50^\circ)$ ,  $\theta_A (= 20^\circ)$ , and angular thickness of the cyclotron emission region ( $\theta_1 = 10^\circ$  and  $\theta_2 = 12^\circ$ ).

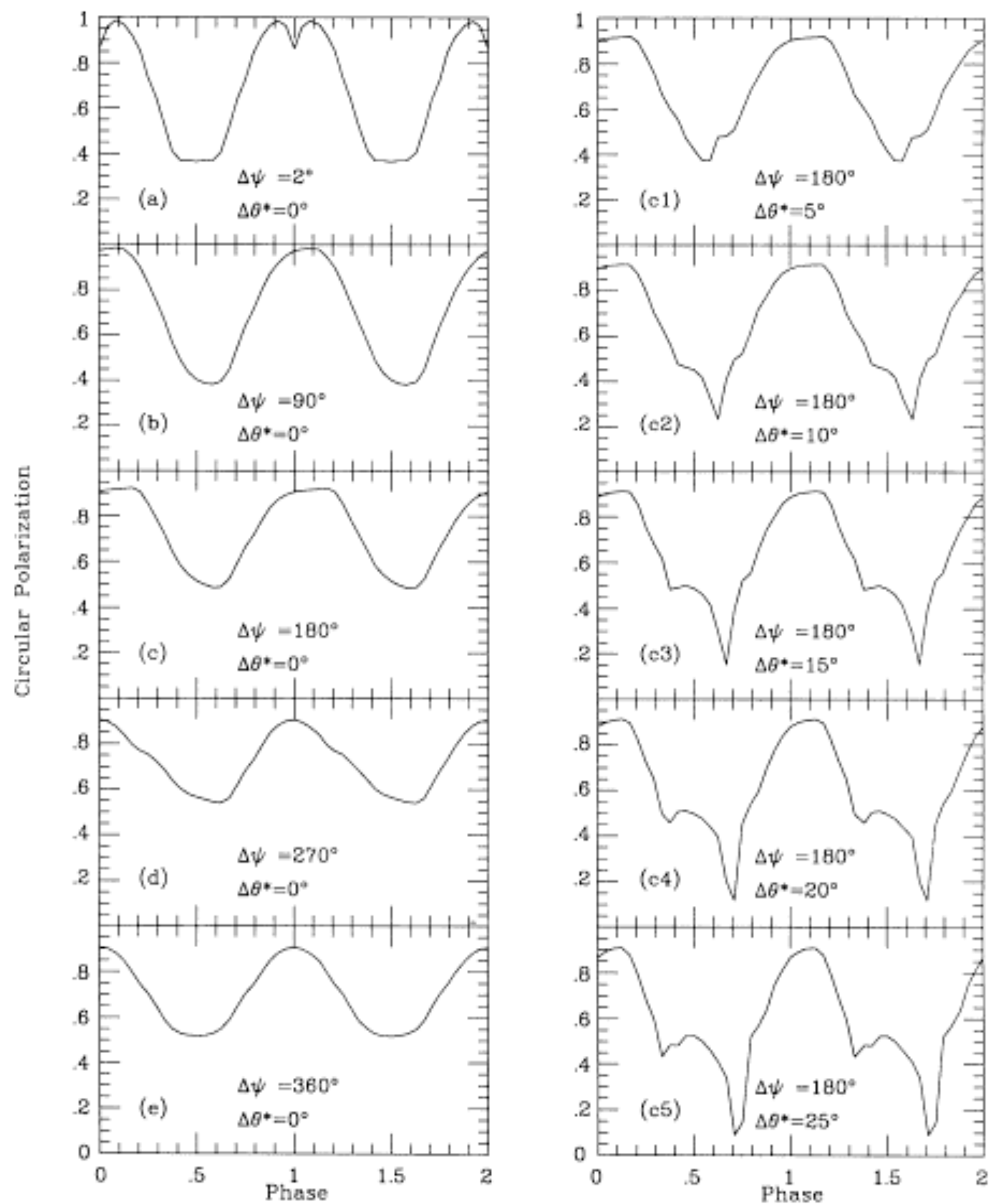


FIG. 4

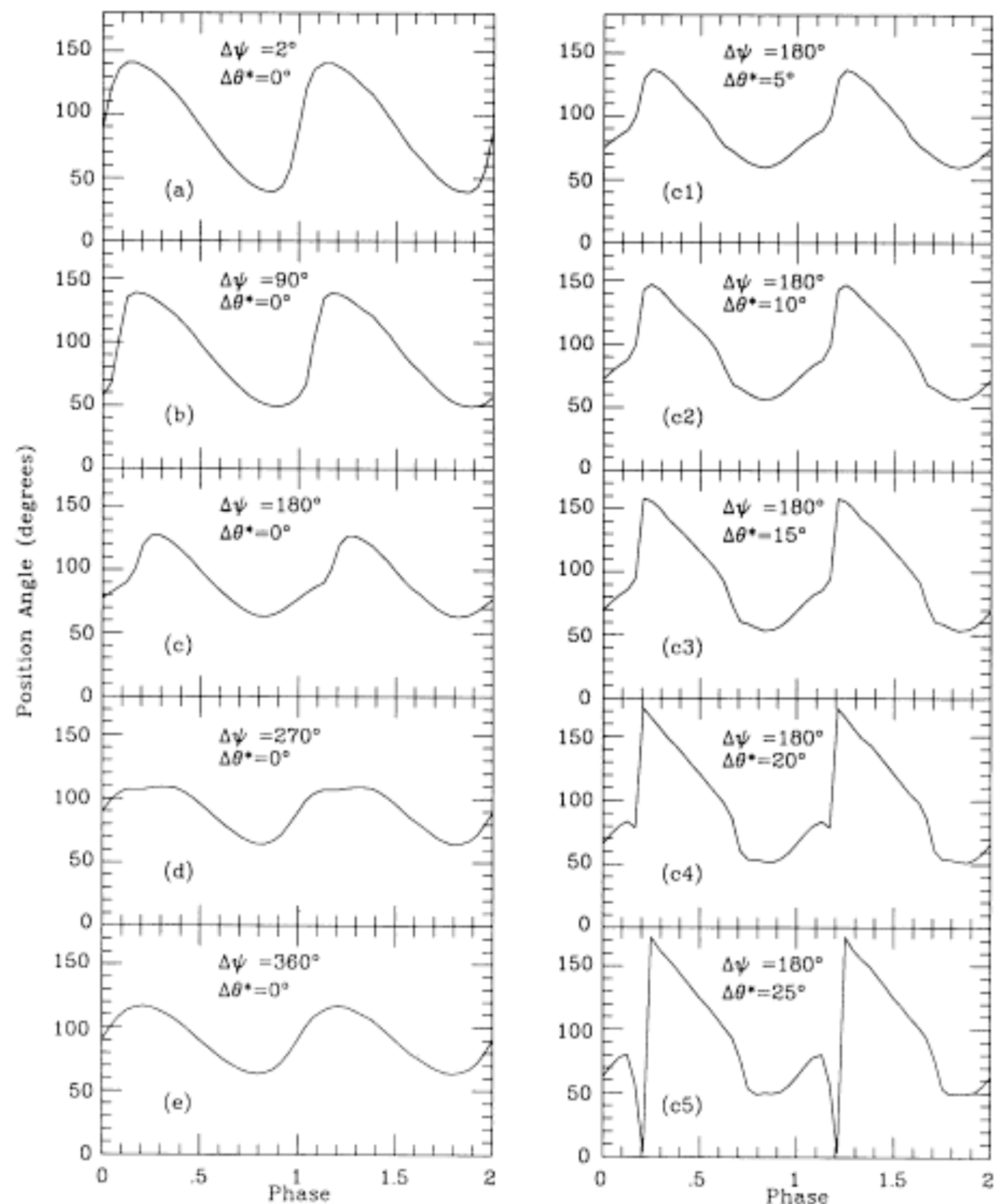
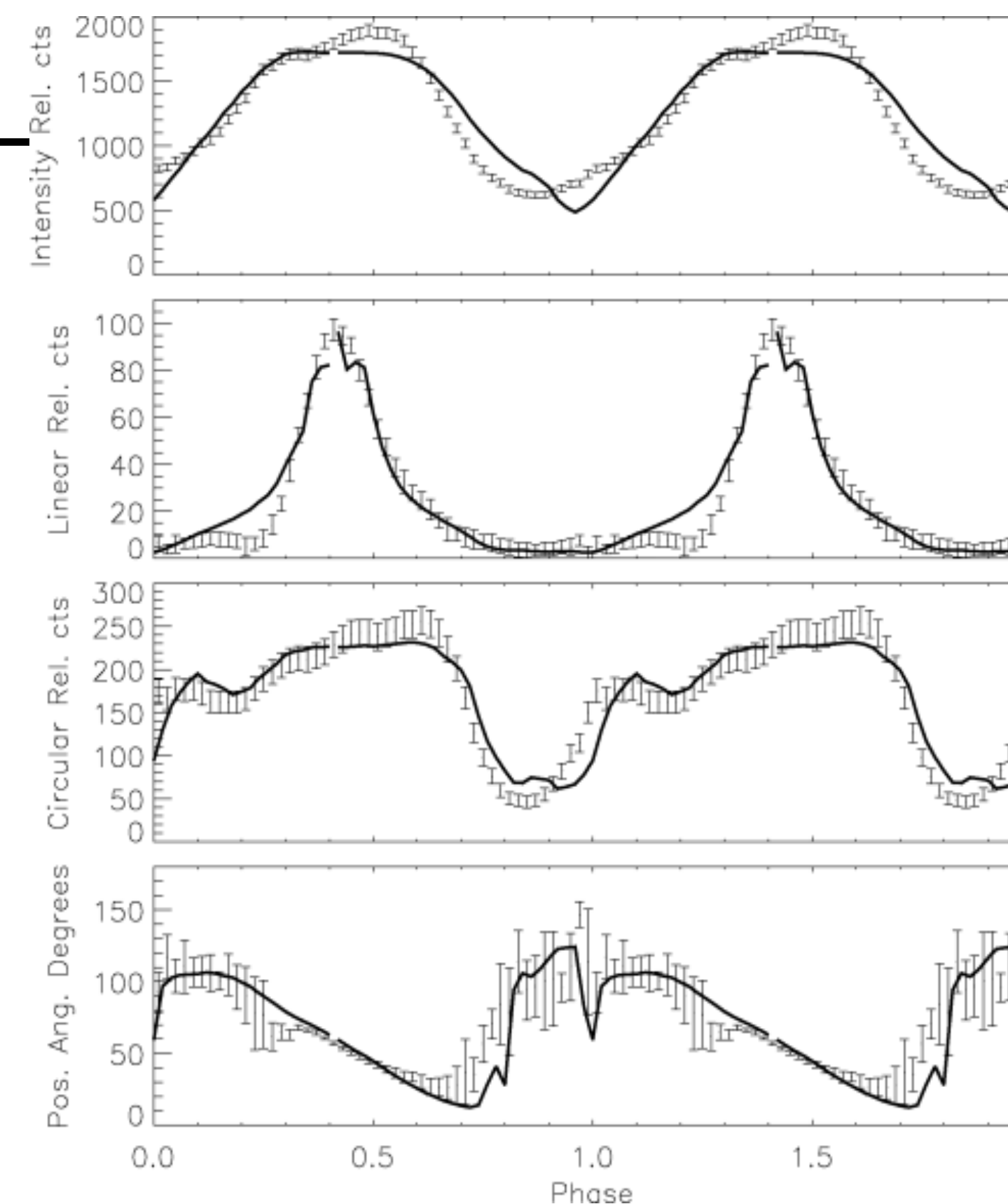


FIG. 5

FIG. 4.—Theoretical circular polarization curves obtained for fixed values of  $i = 50^\circ$ ,  $\theta_A = 20^\circ$  and angular thickness of the cyclotron emission region ( $\theta_1 = 10^\circ$  and  $\theta_2 = 12^\circ$ ).  
 FIG. 5.—Theoretical position angle curves obtained for fixed values of  $i = 50^\circ$ ,  $\theta_A = 20^\circ$ , and angular thickness of the cyclotron emission region ( $\theta_1 = 10^\circ$  and  $\theta_2 = 12^\circ$ ).

# EXTENDED REGIONS

- Potter, Hakala & Cropper (1998, MNRAS, 297, 1261)
  - ❖ extended and no-homogeneous region
    - ◆ sum of points with physical properties arbitrarily chosen in order to reproduce the observations (2D)
  - ❖ WM85 is the basic model
  - ❖ genetic algorithm to fit the data
  - ❖ applications and improvements on subsequent articles



- Potter et al. (2004, MNRAS, 348, 316)

- ❖ Application to V834 Cen
- ❖ Data from Schwope et al. (1993)
- ❖ One band fitting

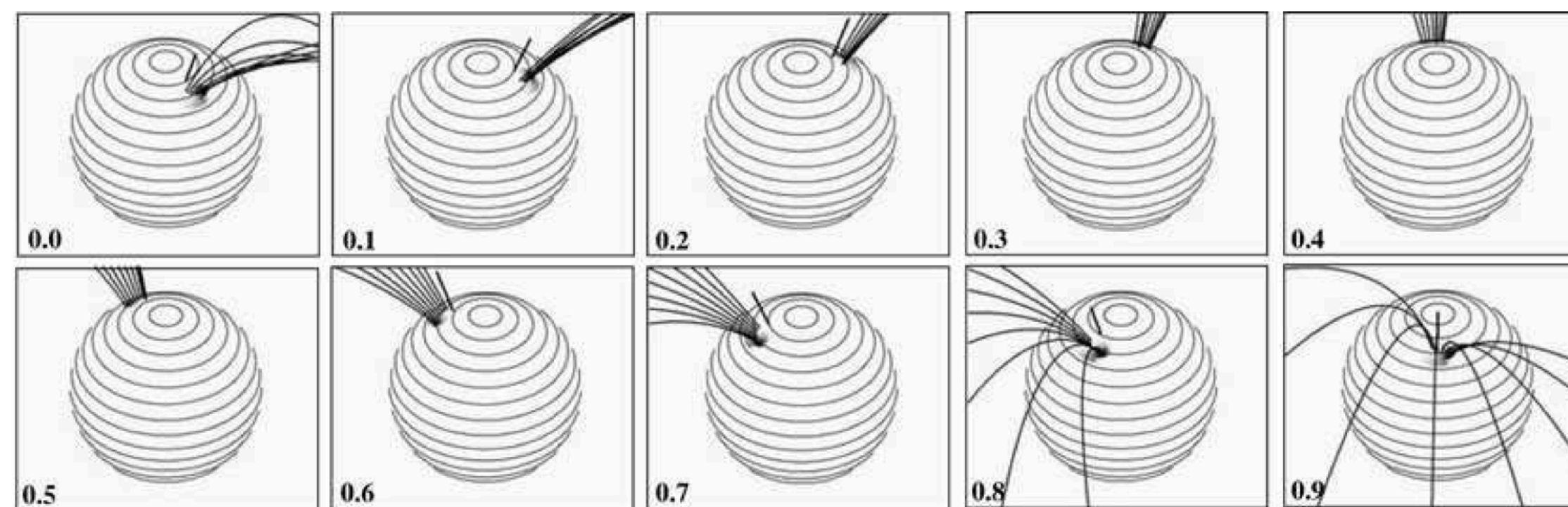


**Figure 2.** View from the Earth of the white dwarf in V834 Cen for a complete orbital rotation. The predicted cyclotron emission region is shown as the (small) grey-scale region. The magnetic pole is indicated by a short solid line at latitude 10 degrees from the spin pole. Latitudes are indicated every 10 degrees. Magnetic field lines (see Section 4.1) are shown as solid lines.



A code to model optical and X-ray emission of polars

- Post-shock region modelling
  - ❖ radiative transfer
    - ◆ cyclotron (optical emission)
    - ◆ bremsstrahlung (X-rays)
    - ◆ 3D region
  - ❖ solution of physical properties along the magnetic accretion column
    - ◆ density and temperatures profiles

Costa & CVR 2009, MNRAS, 398, 240

Silva, CVR + 2013, MNRAS, 432, 1587

Belloni, CVR+2021, ApJS, 256, 45

# POST-SHOCK STRUCTURE PROBLEM

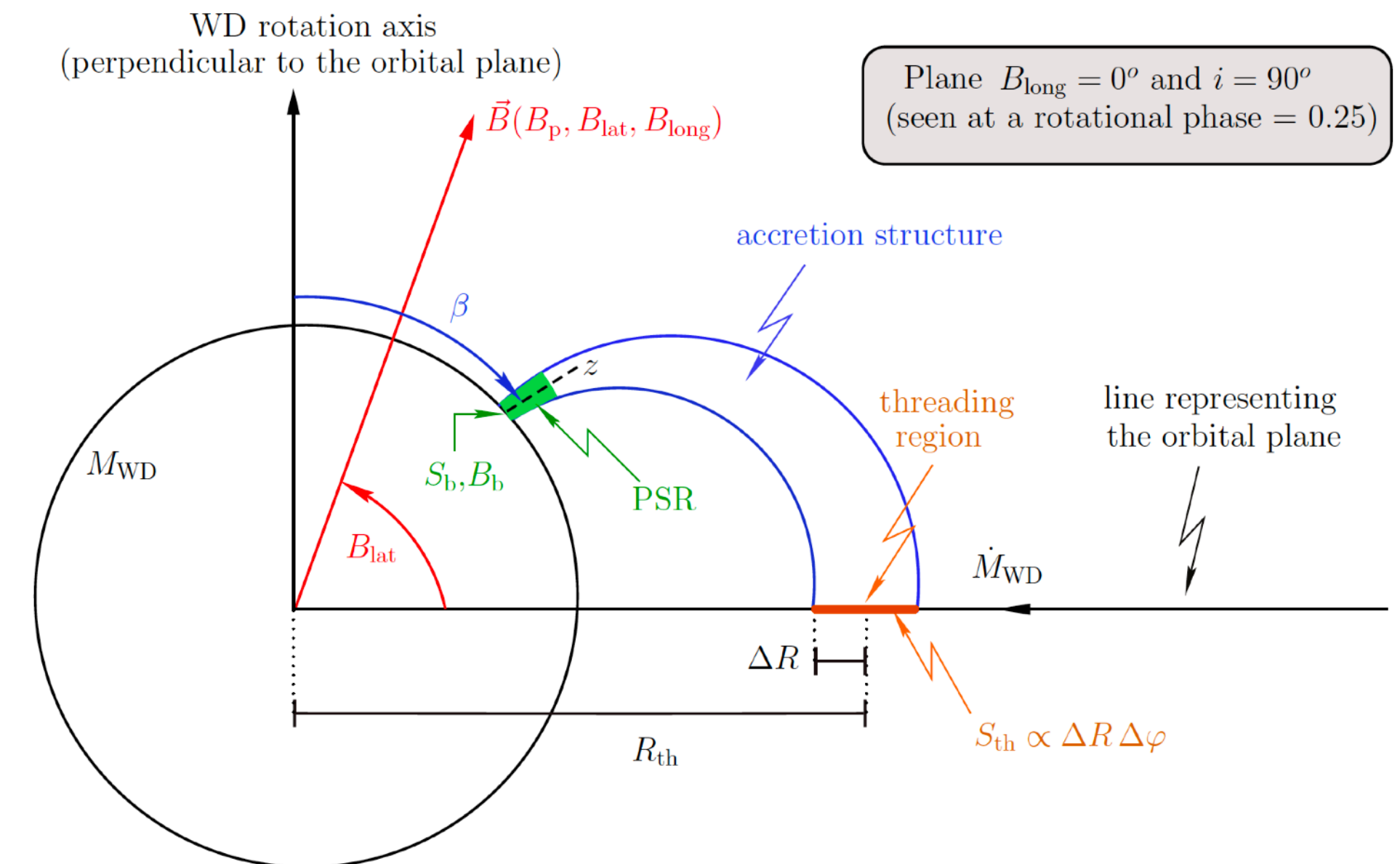
- Solution of the temperature and density profiles in the post-shock region

$$\frac{d}{dz} (S\rho v) = 0,$$

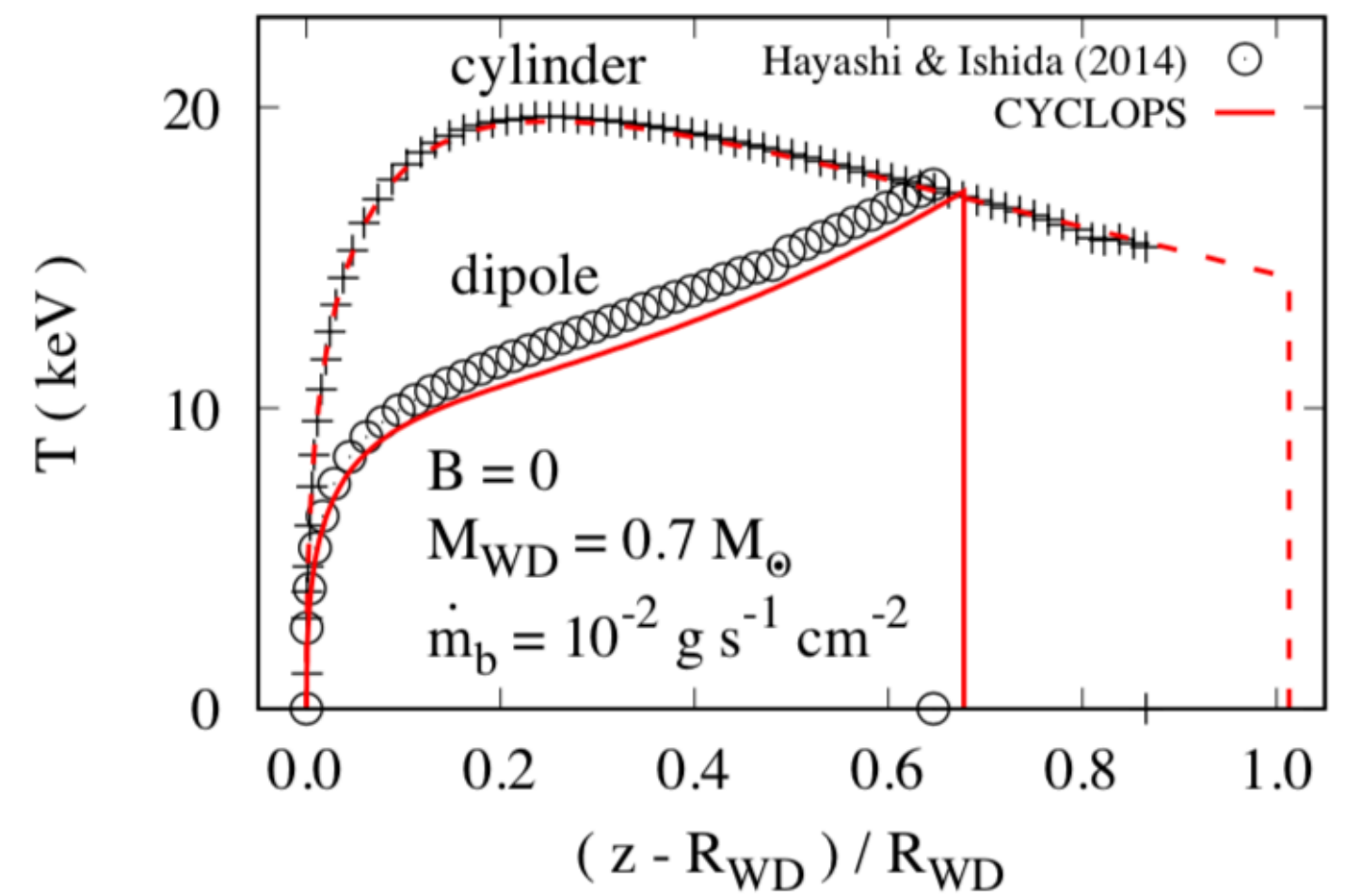
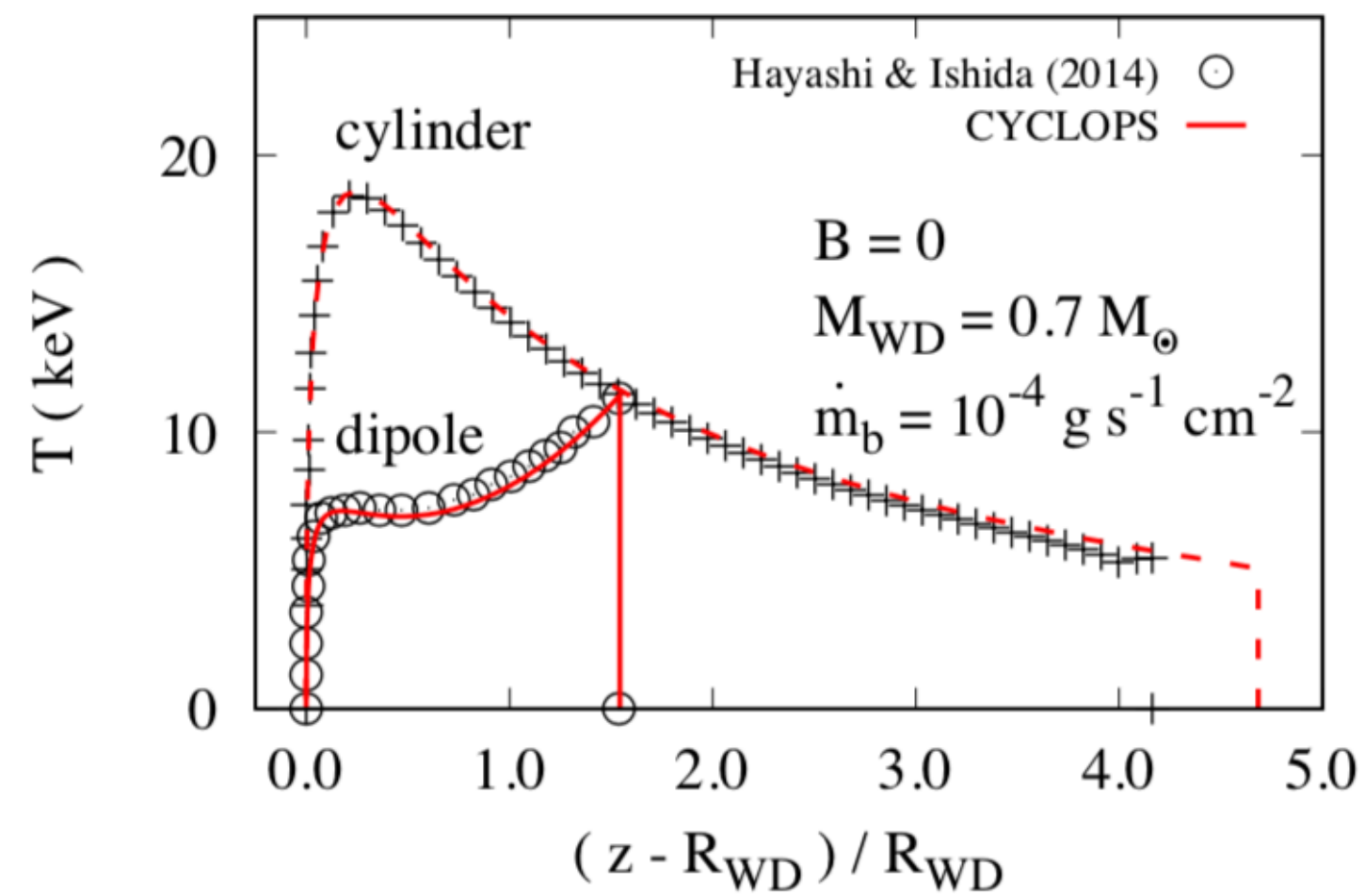
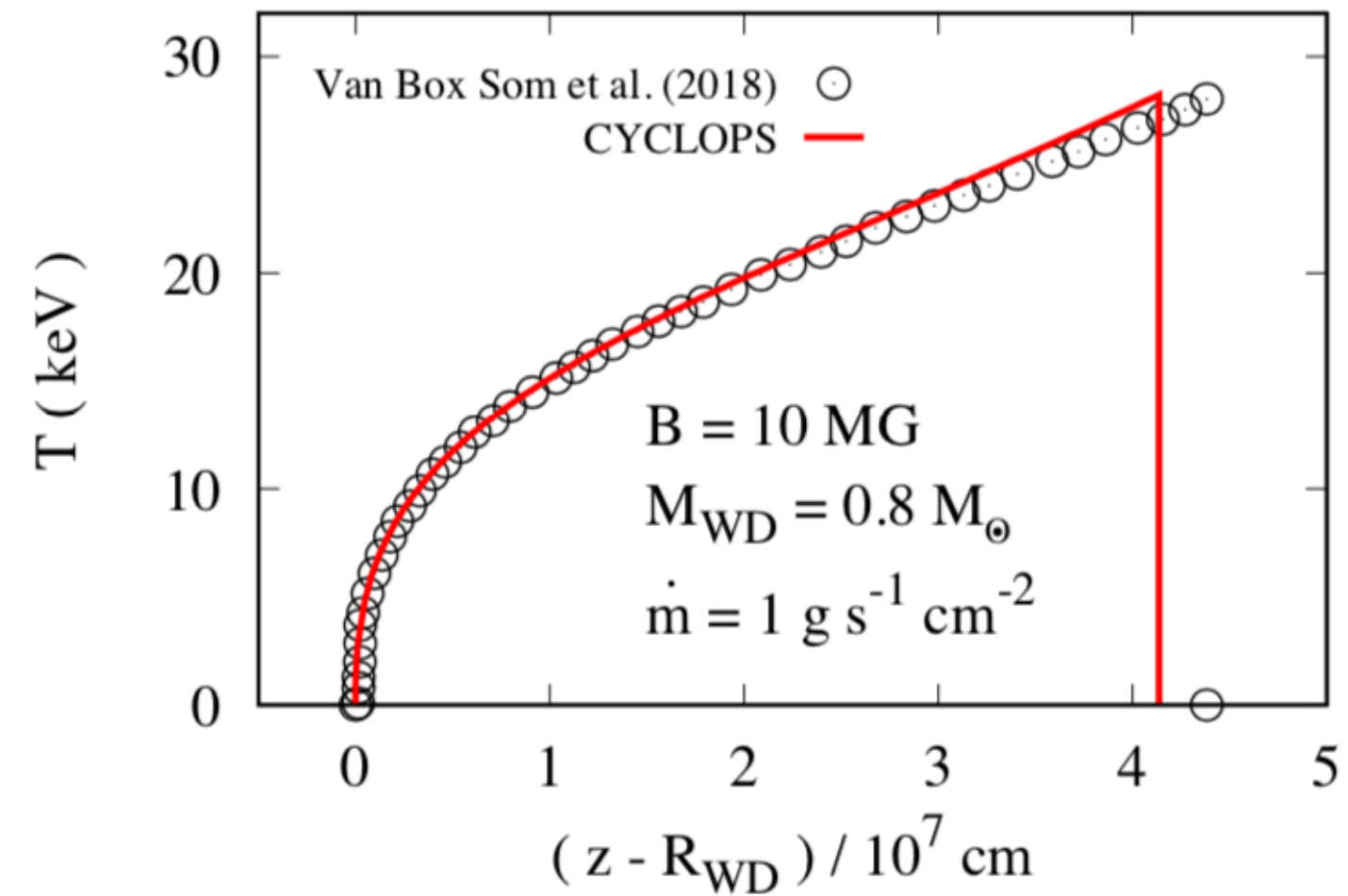
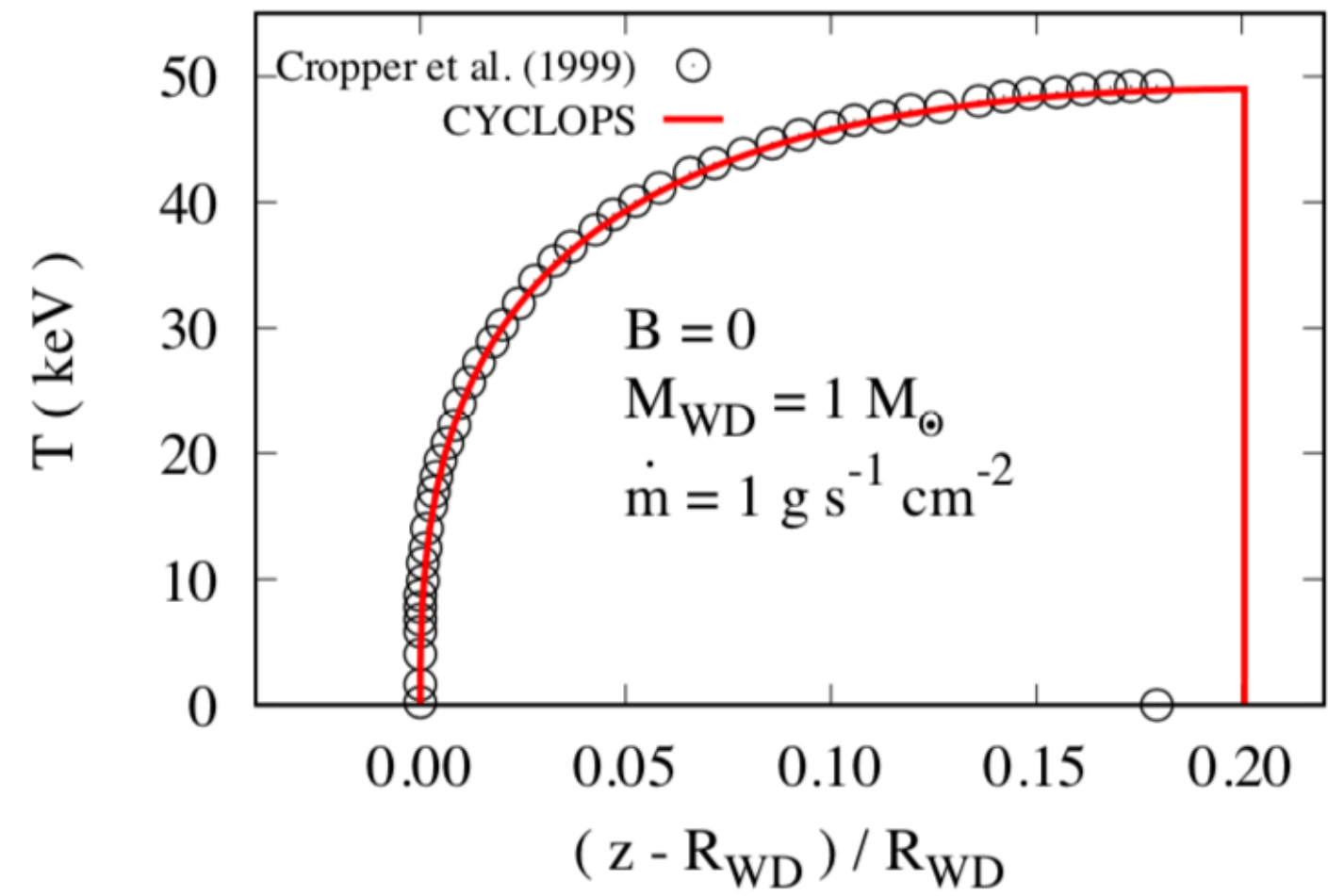
$$\frac{d}{dz} (\rho v^2 + P) + \frac{\rho v^2}{S} \frac{dS}{dz} + \rho g_{\text{WD}} = 0,$$

$$v \frac{dP}{dz} + \gamma P \frac{dv}{dz} + (\gamma - 1) \left( \Lambda - \frac{\rho v^3}{2S} \frac{dS}{dz} \right) = 0,$$

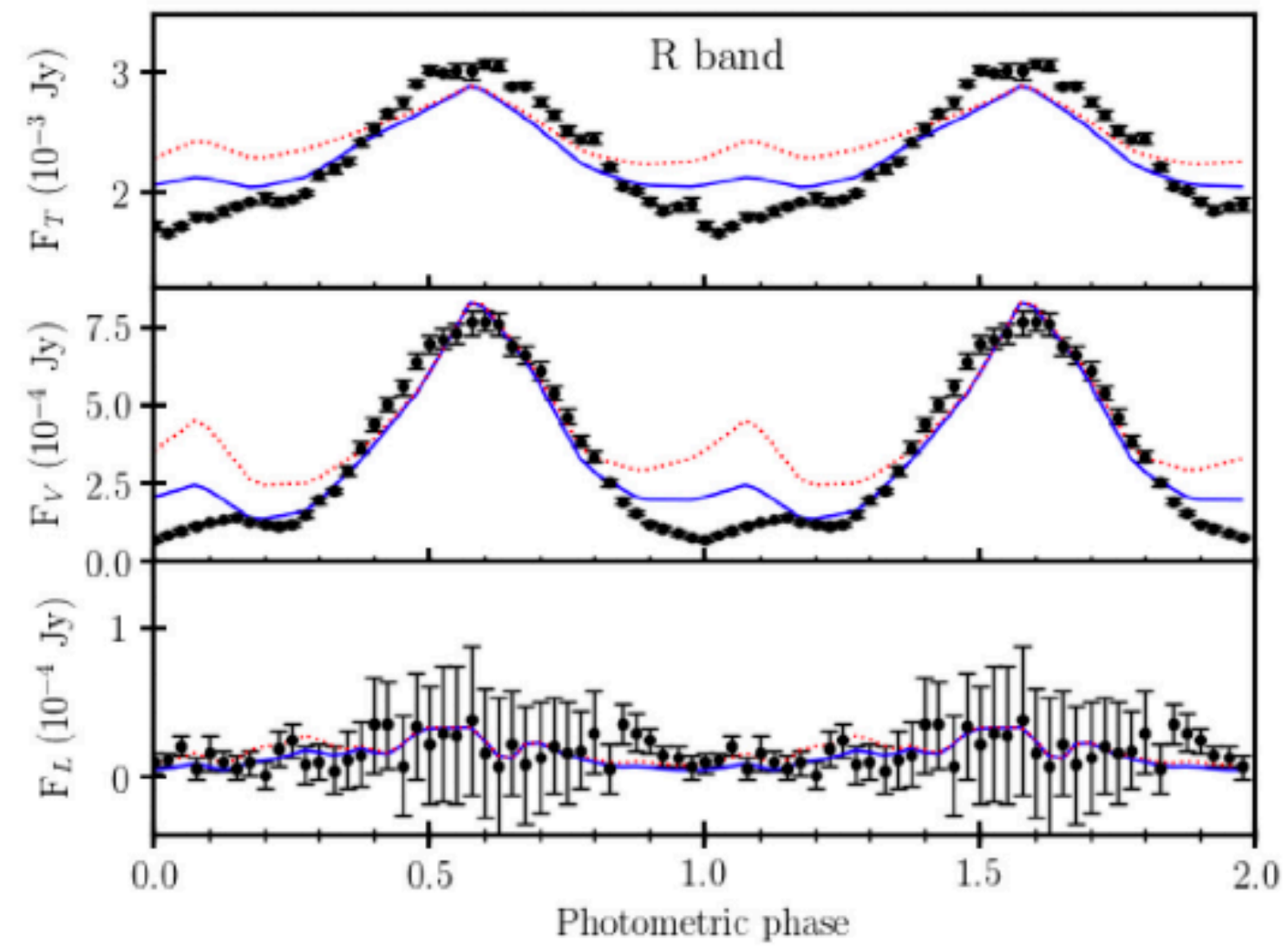
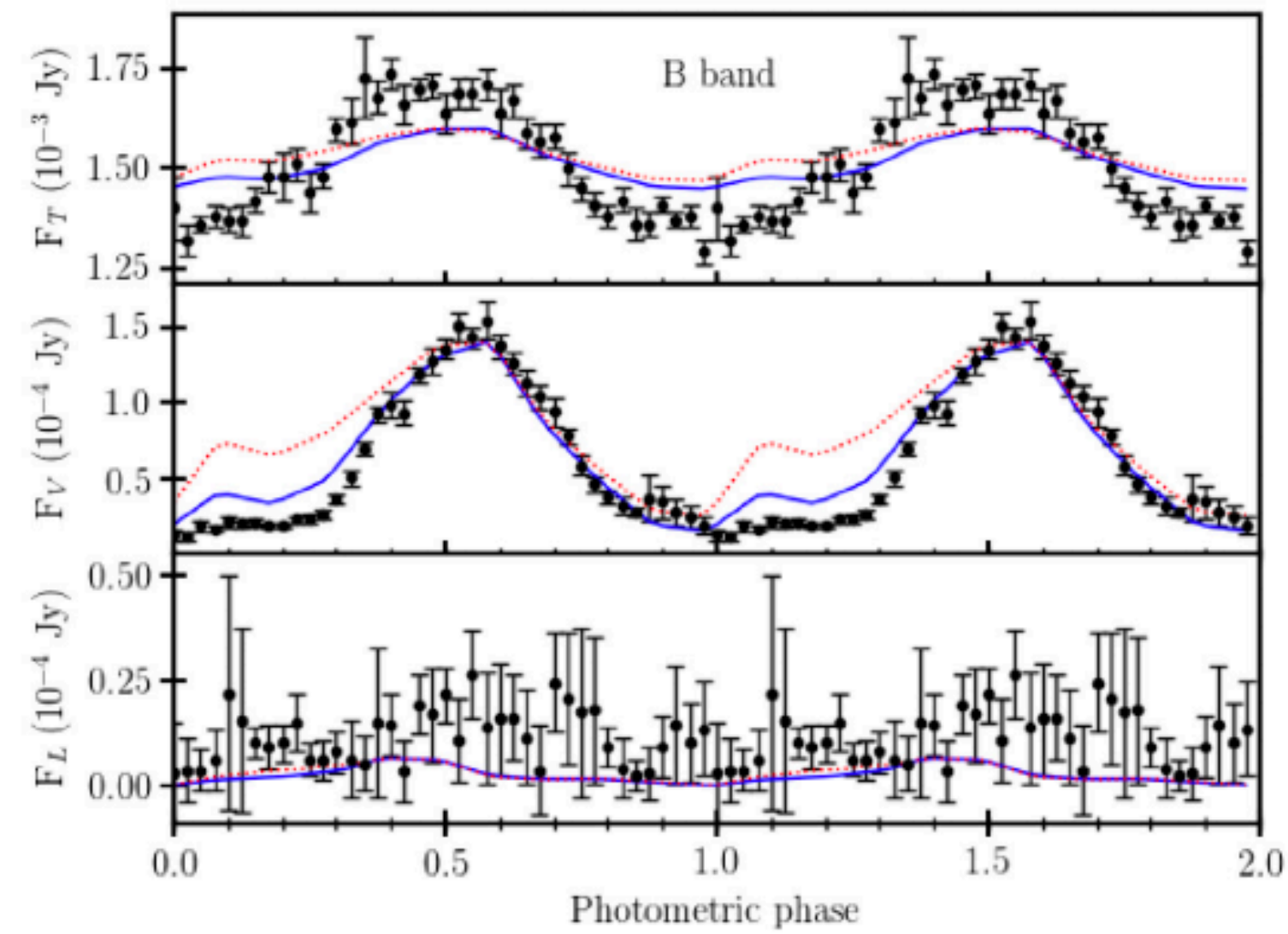
Belloni, CVR+ 2021, ApJS, 256, 45



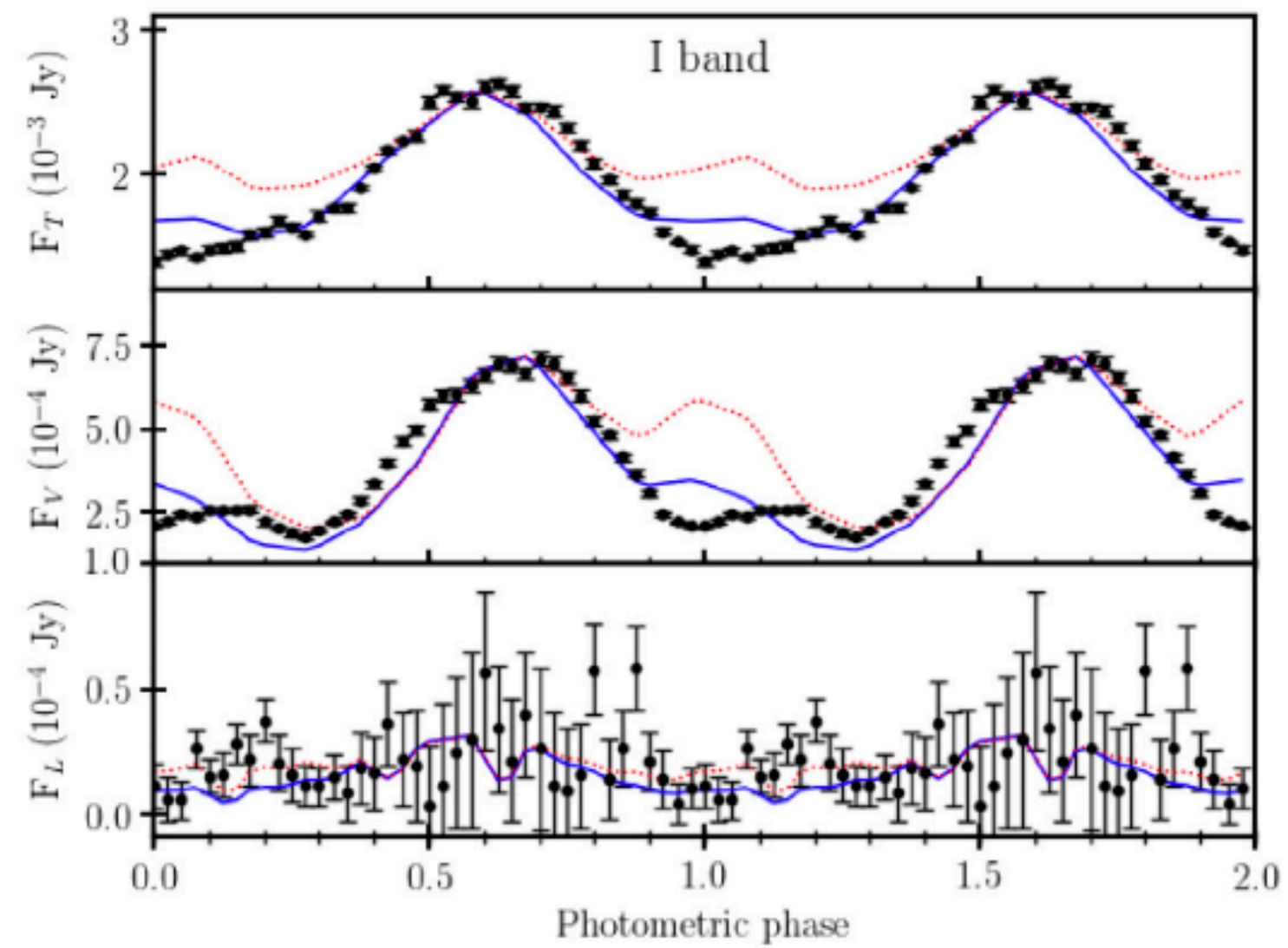
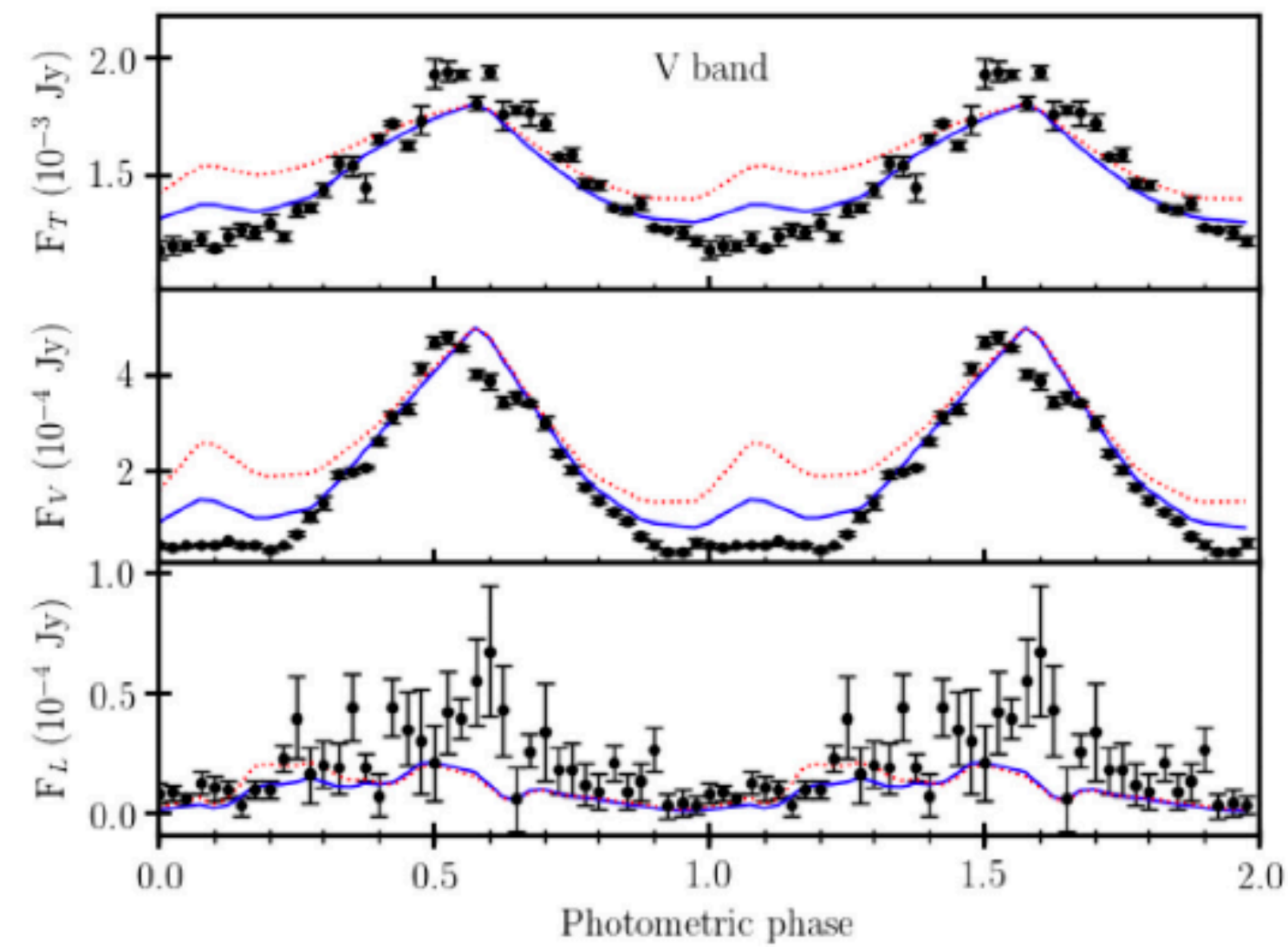
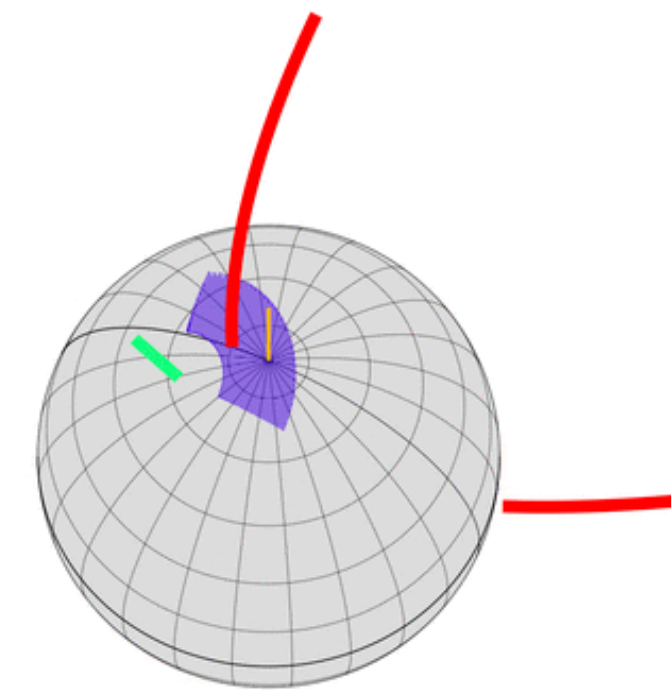
# POST-SHOCK SOLUTION VS PREVIOUS RESULTS



# V348 PAV



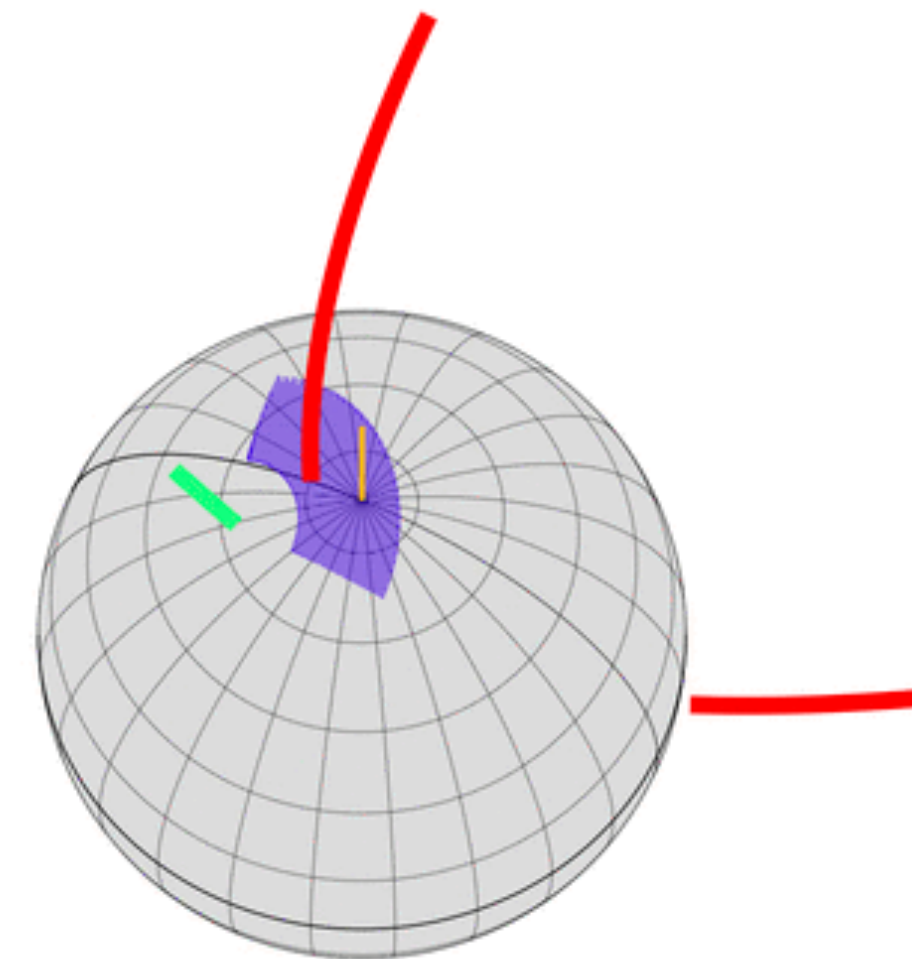
Model: blue line



Oliveira, CVR+ 2019, MNRAS, 489, 4032

**Table 2.** Physical and geometrical properties of V348 Pav estimated from CYCLOPS modelling.

CYCLOPS input parameters	Fitted values
White dwarf mass, $M_{\text{WD}}$	$0.85 M_{\odot}$
Mass accretion rate, $\dot{M}$	$10^{-11} M_{\odot} \text{ yr}^{-1}$
Magnetic field intensity in the pole, $B_{\text{pole}}$	$28 \times 10^6 \text{ G}$
Latitude of the magnetic axis, $B_{\text{lat}}$	$67^{\circ}$
Longitude of the magnetic axis, $B_{\text{long}}$	$31^{\circ}$
Orbital inclination, $i$	$25^{\circ}$
Colatitude of the PSR, $\beta$	$10^{\circ}$
Azimuthal semi-extension of the threading region	$54^{\circ}$
Radial semi-extension of the threading region	0.7
CYCLOPS model associated and resulting quantities	
	Values
Specific accretion rate, $a$ , in the WD surface	$0.0065 \text{ g cm}^{-2} \text{ s}^{-1}$
Height of the PSR, $h$	$0.016 R_{\text{WD}}$
Shock electronic temperature	37 keV
Shock electronic number density	$4 \times 10^{13} \text{ cm}^{-3}$
Shock electronic mass density	$4 \times 10^{-11} \text{ g cm}^{-3}$
Size in latitude of the PSR footprint	$19^{\circ}$
Footprint area relative to the WD surface	0.017
Distance of the threading region to the WD centre	$12 R_{\text{WD}}$
Magnetic field in the PSR	24–27 MG
Phase shift applied to the model, $\delta_{\text{phase}}$	-0.317
Added flux in $B$ band	0.0014 Jy
Added flux in $V$ band	0.0012 Jy
Added flux in $R$ band	0.0018 Jy
Added flux in $I$ band	0.0012 Jy



# V348 PAV

Oliveira, CVR+ 2019, MNRAS, 489, 4032

**Table 2.** Physical and geometrical properties of V348 Pav estimated from CYCLOPS modelling.

CYCLOPS input parameters	Fitted values
White dwarf mass, $M_{\text{WD}}$	$0.85 M_{\odot}$
Mass accretion rate, $\dot{M}$	$10^{-11} M_{\odot} \text{ yr}^{-1}$
Magnetic field intensity in the pole, $B_{\text{pole}}$	$28 \times 10^6 \text{ G}$

**White dwarf mass,  $M_{\text{WD}}$**

**Mass accretion rate,  $\dot{M}$**

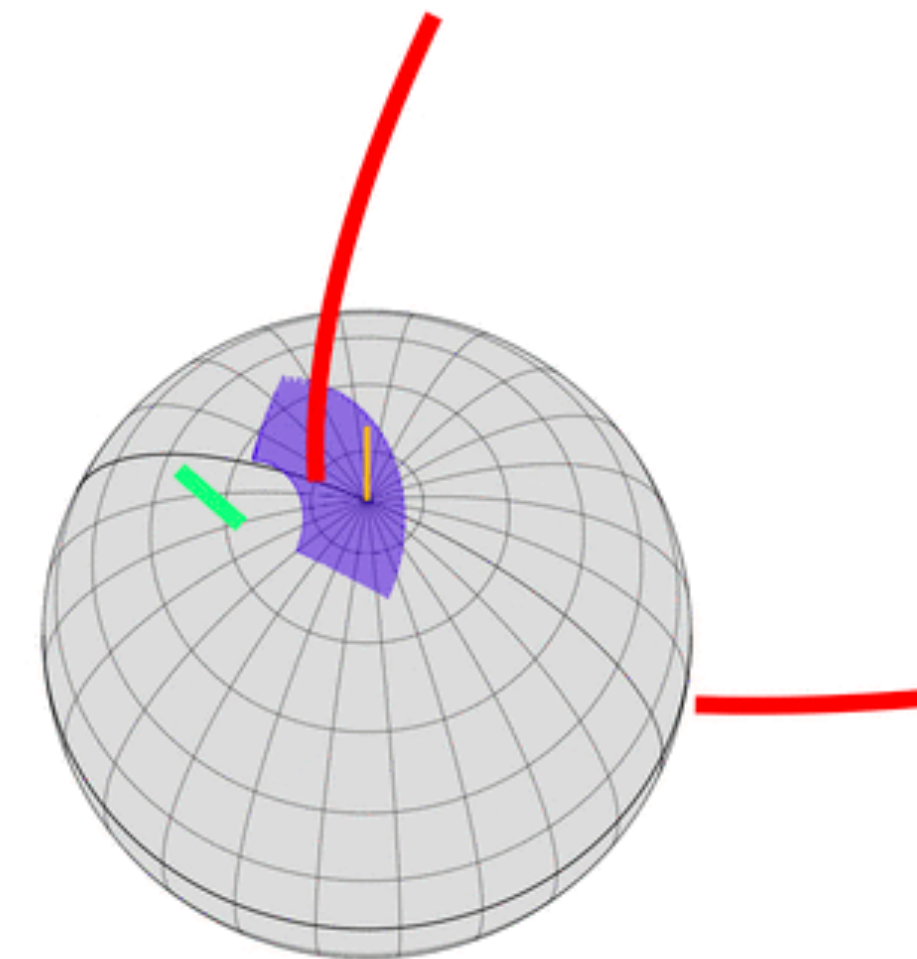
**Magnetic field intensity in the pole,  $B_{\text{pole}}$**

**$0.85 M_{\odot}$**

**$10^{-11} M_{\odot} \text{ yr}^{-1}$**

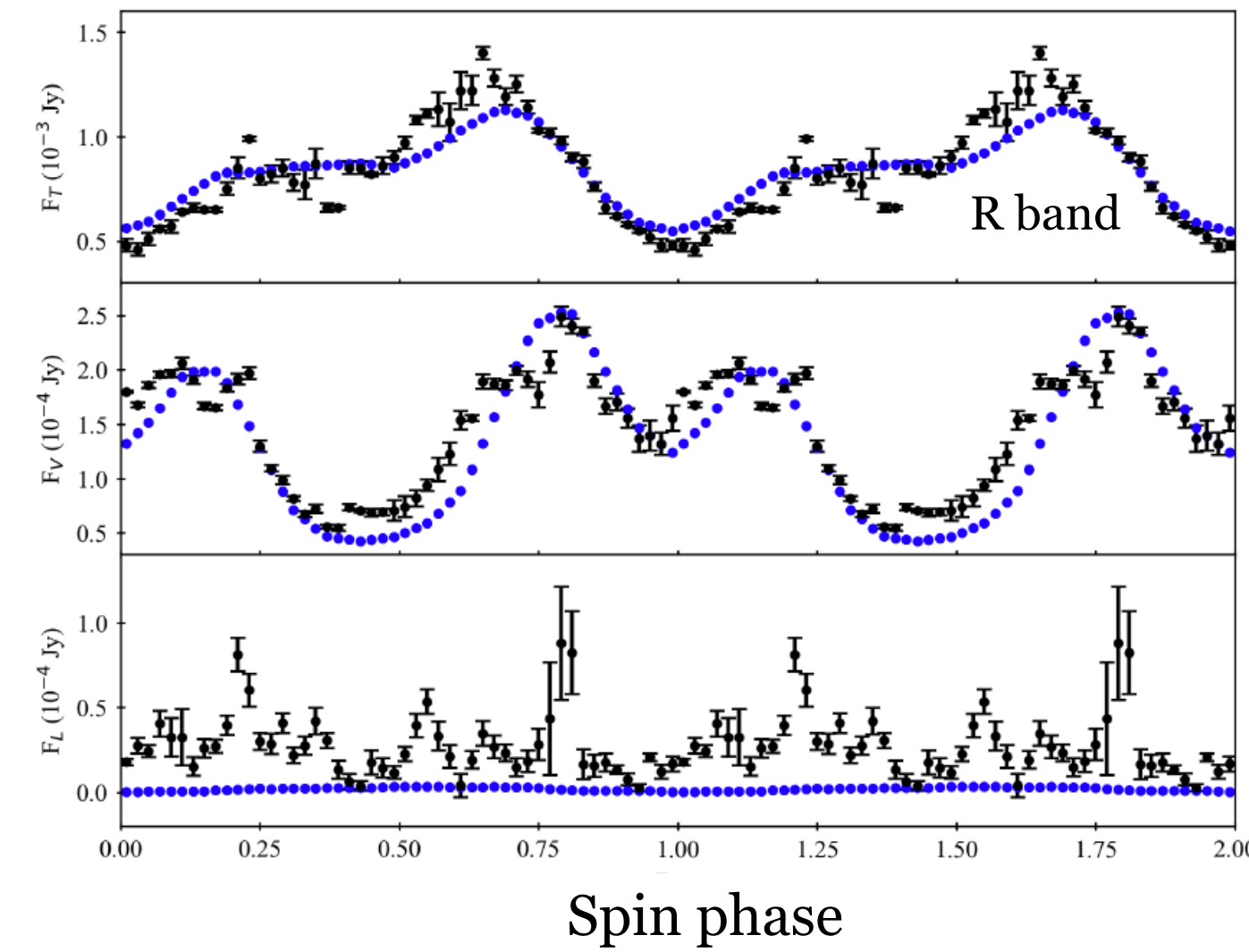
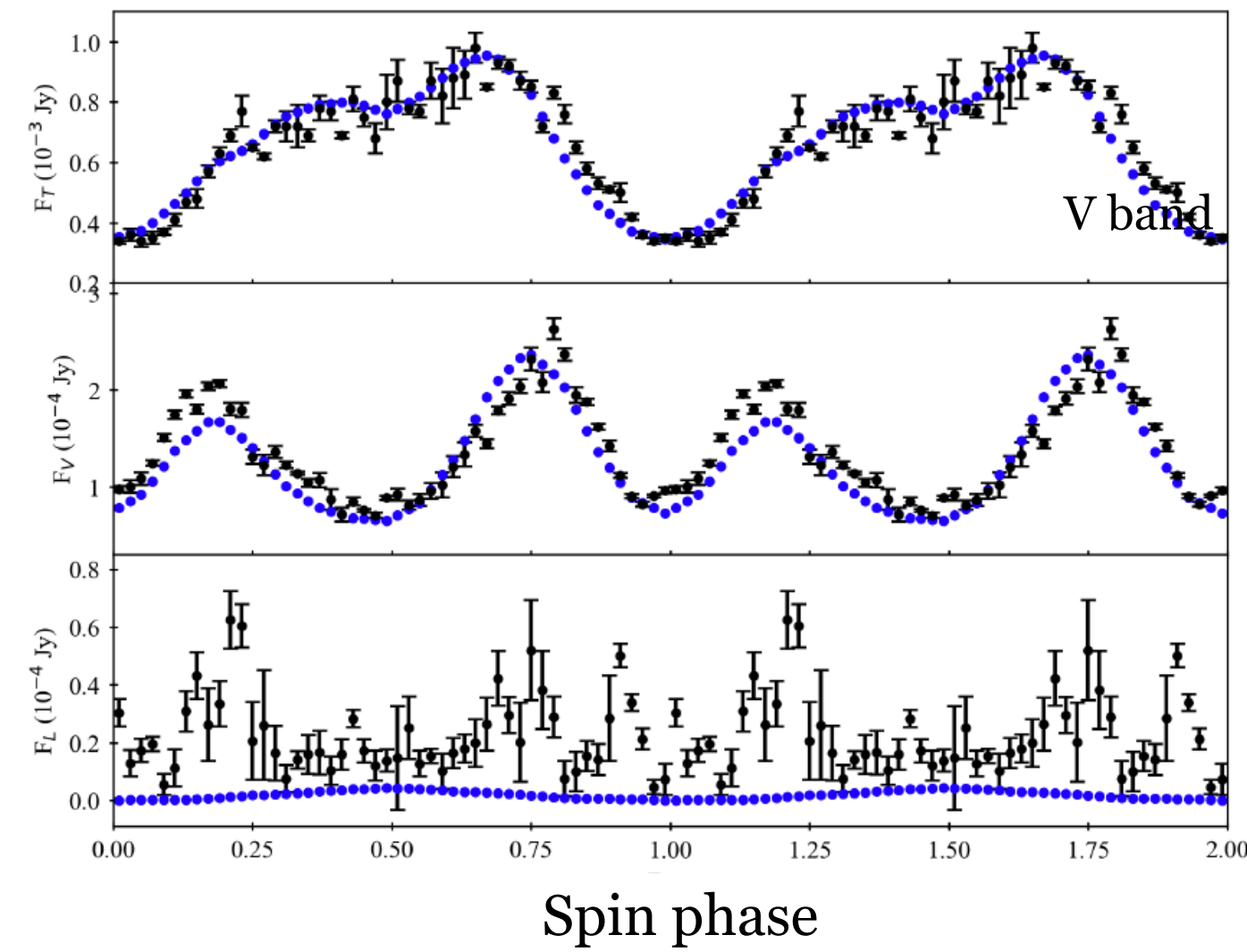
**$28 \times 10^6 \text{ G}$**

CYCLOPS model associated and resulting quantities	Values
Specific accretion rate, $a$ , in the WD surface	$0.0065 \text{ g cm}^{-2} \text{ s}^{-1}$
Height of the PSR, $h$	$0.016 R_{\text{WD}}$
Shock electronic temperature	$37 \text{ keV}$
Shock electronic number density	$4 \times 10^{13} \text{ cm}^{-3}$
Shock electronic mass density	$4 \times 10^{-11} \text{ g cm}^{-3}$
Size in latitude of the PSR footprint	$19^{\circ}$
Footprint area relative to the WD surface	$0.017$
Distance of the threading region to the WD centre	$12 R_{\text{WD}}$
Magnetic field in the PSR	$24\text{--}27 \text{ MG}$
Phase shift applied to the model, $\delta_{\text{phase}}$	$-0.317$
Added flux in $B$ band	$0.0014 \text{ Jy}$
Added flux in $V$ band	$0.0012 \text{ Jy}$
Added flux in $R$ band	$0.0018 \text{ Jy}$
Added flux in $I$ band	$0.0012 \text{ Jy}$

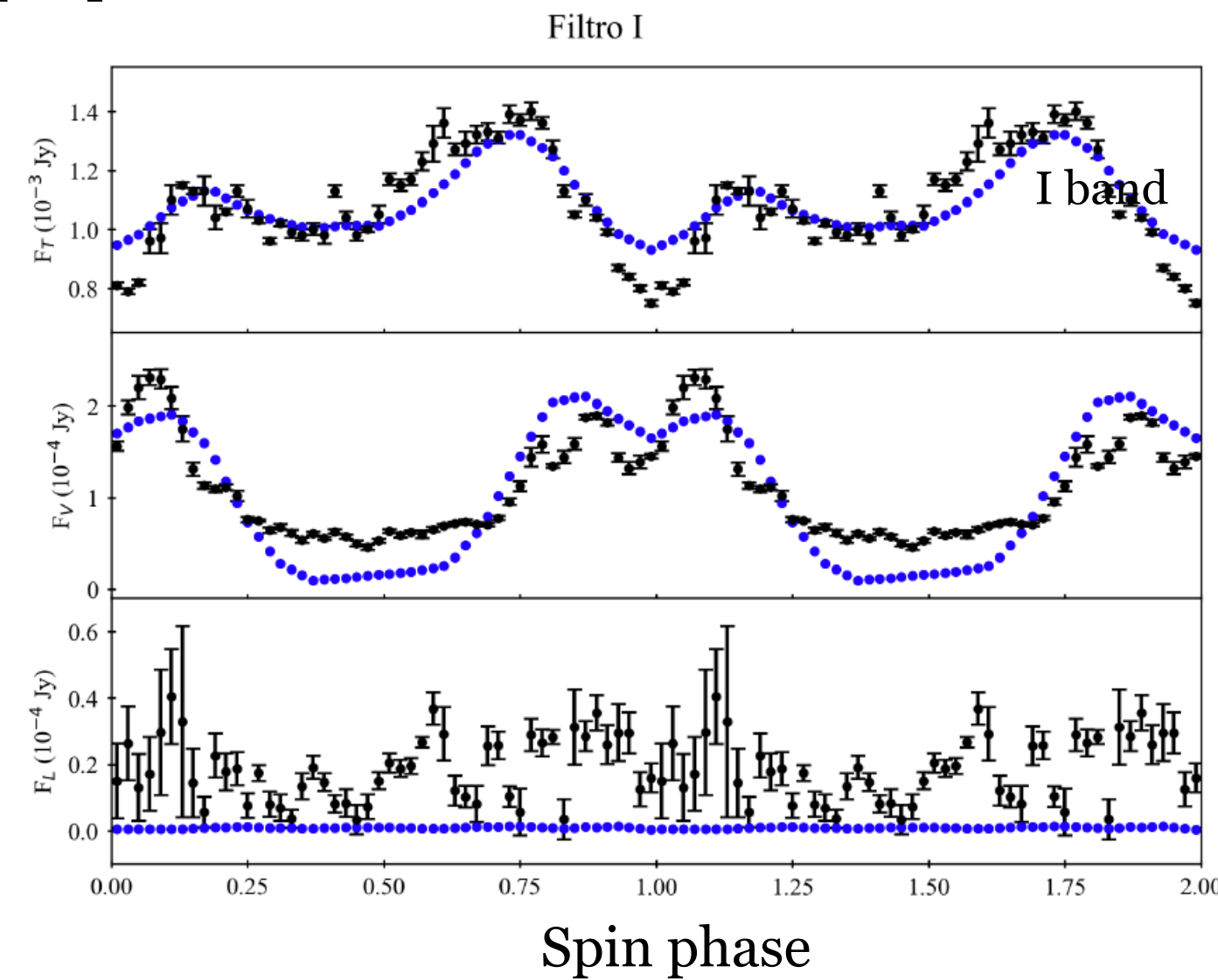


# 1RXS J174320.1-042953

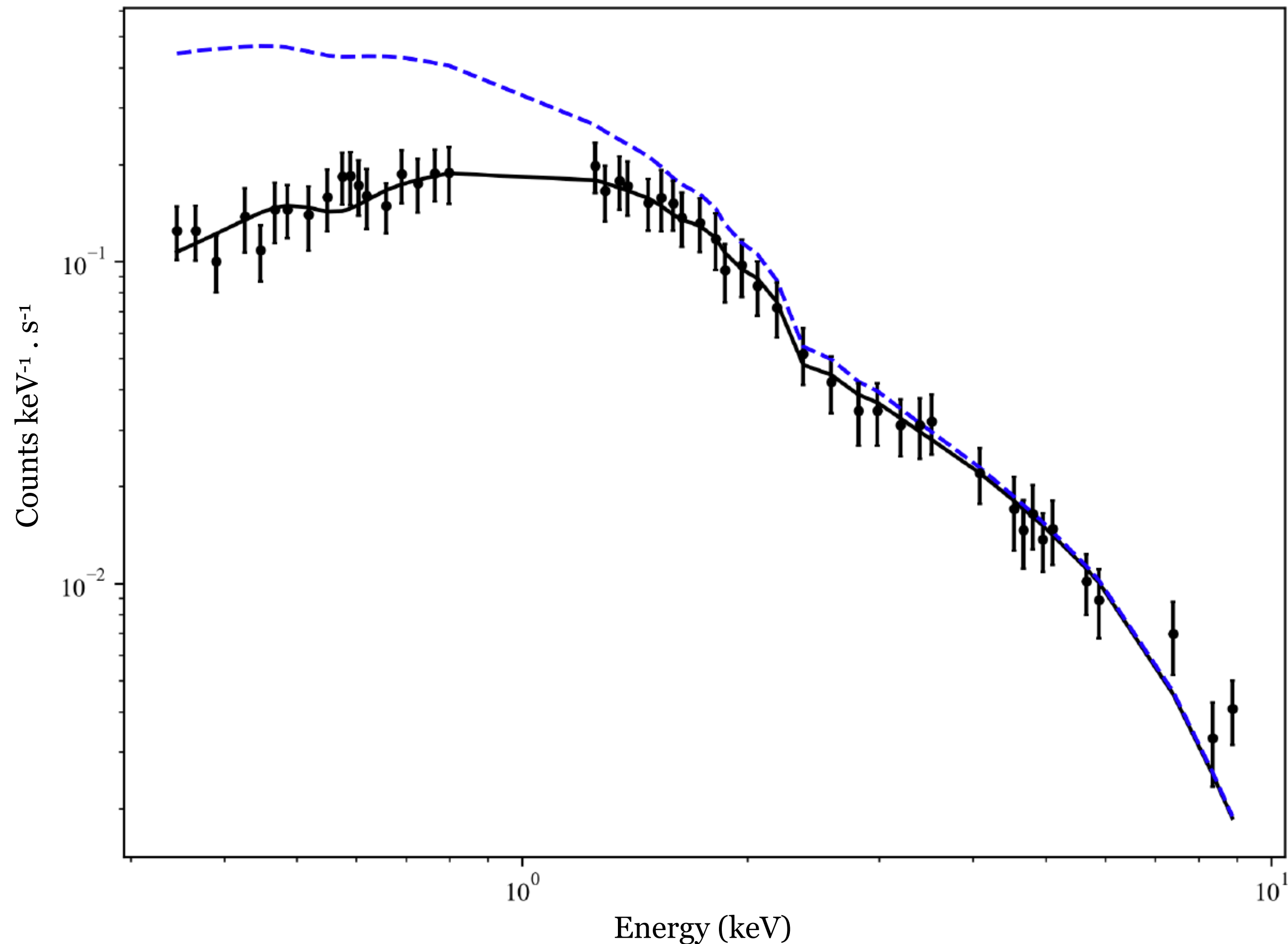
Martins' thesis 2022



Black: data  
Blue: Model



Preliminary results of optical data modelling



- Our aim is to model simultaneously X-ray and optical data
- Preliminary fittings indicate a massive WD:
  - ❖  $\sim 1.3 M_{\text{sun}}$

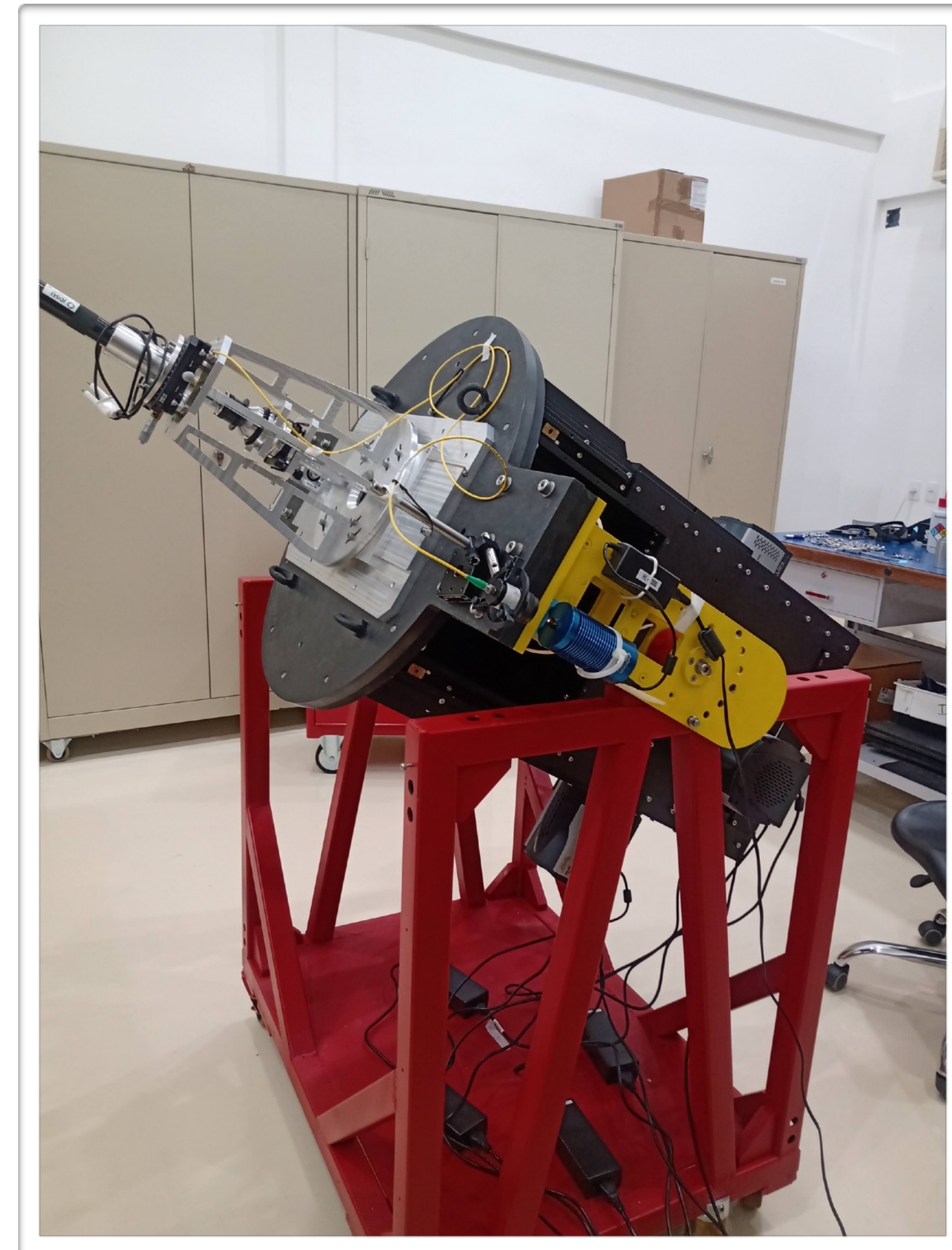
Preliminary modelling of XMM data

# SPARC4

## Simultaneous Polarimeter and Rapid Camera in 4 bands

A new instrument to  
study CVs

- Simultaneous acquisition of four images (griz SDSS bands)
- Many operation modes
  - ❖ imager
  - ❖ polarimeter - linear polarization
  - ❖ polarimeter - linear and circular polarization
- 1.6m telescope of Observatório do Pico dos Dias/Brazil
- First light planned to November/2022.



See poster 144

# CONCLUSIONS

---

- CVs can show optical polarization that, when present, reveals magnetic accretion onto the white dwarf.
- The radiation from the post-shock region is responsible by the observed polarization and X-ray emission of magnetic CVs.
- To model the observations, a proper solution of the physical quantities in the post-shock region is necessary.
- Cyclops is a tool to model optical and X-ray emission from magnetic CVs.

Acknowledgements

Fapesp: 2022/06658-7  
Finep: Proc. 0/1/16/0076/00  
CNPq: Proc. 310930/2021-9

# POST-SHOCK STRUCTURE PROBLEM

Belloni, CVR+ 2021

$$\frac{d}{dz}(S\rho v) = 0,$$

$$\frac{d}{dz}(\rho v^2 + P) + \frac{\rho v^2}{S} \frac{dS}{dz} + \rho g_{\text{WD}} = 0,$$

$$v \frac{dP}{dz} + \gamma P \frac{dv}{dz} + (\gamma - 1) \left( \Lambda - \frac{\rho v^3}{2S} \frac{dS}{dz} \right) = 0,$$

$$g_{\text{WD}}(z) = \frac{GM_{\text{WD}}}{z^2}$$

$$S(z) \rho(z) v(z) = S(z) \dot{m}(z) = \dot{M}_{\text{WD}}$$

$$S(z) = S_b \left( \frac{z}{R_{\text{WD}}} \right)^n$$

Boundary conditions

$$\left\{ \begin{array}{l} v_{\text{sh}} = 0.25 \sqrt{2GM_{\text{WD}} (1/z_{\text{sh}} - 1/R_{\text{th}})}, \\ \rho_{\text{sh}} = \dot{m}_{\text{sh}} / v_{\text{sh}}, \\ P_{\text{sh}} = 3 \dot{m}_{\text{sh}} v_{\text{sh}}, \\ T_{\text{sh}} = 3 \mu m_H v_{\text{sh}}^2 / k_B, \end{array} \right.$$

